

Sources of Submicrometre Particles Near a Major International Airport

**Mauro Masiol^{1,2}, Roy M. Harrison^{1*†},
Tuan V. Vu¹, David C.S. Beddows¹**

**¹ Division of Environmental Health and Risk Management,
School of Geography, Earth and Environmental Sciences
University of Birmingham
Edgbaston, Birmingham B15 2TT
United Kingdom**

**² Division of Epidemiology, Department of Public Health
Sciences, University of Rochester Medical Center,
265 Crittenden Boulevard, CU 420644
Rochester, NY 14642, United States**

* To whom correspondence should be addressed.

Tele: +44 121 414 3494; Fax: +44 121 414 3709; Email: r.m.harrison@bham.ac.uk

†Also at: Department of Environmental Sciences / Center of Excellence in Environmental Studies, King Abdulaziz University, PO Box 80203, Jeddah, 21589, Saudi Arabia

31 **ABSTRACT**

32 The international airport of Heathrow is a major source of nitrogen oxides, but its contribution to
33 the levels of submicrometre particles is unknown, and is the objective of this study. Two sampling
34 campaigns were carried out during warm and cold seasons at a site close to the airfield (1.2 km).
35 Size spectra were largely dominated by ultrafine particles: nucleation particles (<30 nm) were found
36 to be ~10 times higher than those commonly measured in urban background environments of
37 London. Five clusters and 6 factors were identified by applying *k*-means cluster analysis and
38 positive matrix factorization (PMF) respectively to particle number size distributions; their
39 interpretation was based on their modal structures, wind directionality, diurnal patterns, road and
40 airport traffic volumes and on the relationship with weather and other air pollutants. Airport
41 emissions, fresh and aged road traffic, urban accumulation mode and two secondary sources were
42 then identified and apportioned. The fingerprint of Heathrow has a characteristic modal structure
43 peaking at <20 nm and accounts for 30-35% of total particles in both the seasons. Other main
44 contributors are fresh (24-36%) and aged (16-21%) road traffic emissions and urban accumulation
45 from London (around 10%). Secondary sources accounted for less than 6% in number
46 concentrations but for more than 50% in volume concentration. The analysis of a strong regional
47 nucleation event showed that both the cluster categorisation and PMF contributions were affected
48 during the first 6 hours of the event. In 2016, the UK government provisionally approved the
49 construction of a third runway; therefore the direct and indirect impact of Heathrow on local air
50 quality is expected to increase unless mitigation strategies are applied successfully.

51

52 **Keywords:** Airport; black carbon; size distributions; source apportionment; ultrafine particles

53

54

55 **1. INTRODUCTION**

56 Emerging markets, developing economies and globalisation have driven a fast and continuing
57 growth of civil aviation in the last decades (Lee et al., 2009); this trend is still growing by ~5.5% y⁻¹
58 (ICAO, 2017). As a consequence, the aircraft and road traffic at airports is also increasing, but the
59 information available on the impact of airport emissions upon air quality at ground level is still
60 inadequate (Webb et al., 2008; Masiol and Harrison, 2014). The quantification of airport impacts on
61 local air quality is complicated by the complexity of multiple mobile and static emission sources,
62 with many airports being located near to major cities, highways or industrial plants. Consequently,
63 the development of successful strategies for emission mitigation and the implementation of
64 measures for air quality improvement to meet regulatory standards require a detailed quantification
65 of the contribution of airport and other emissions to the total air pollution load.

66
67 Biological evidence associates the exposure to ultrafine particles (UFPs, <100 nm) with adverse
68 effects upon human health (e.g., Knibbs et al., 2011; Strak et al., 2012; Ostro et al., 2015; Lanzinger
69 et al., 2016). At the current time, there is still limited knowledge of what specific characteristic or
70 association of characteristics may dominate the particle toxicity, and the consequent health
71 outcomes (Atkinson et al., 2010; Strak et al., 2012, Vu et al., 2015a); nevertheless it is well
72 recognised that UFPs can reach the deepest regions of the lung (Salma et al., 2015) and may have
73 orders of magnitude higher surface area to mass ratios compared to larger particles. They offer
74 more surface for the absorption of volatile and semi-volatile species (Kelly and Fussell, 2012; Strak
75 et al., 2012).

76
77 Several studies have reported large increases of UFPs near airports (e.g., Westerdahl et al., 2008;
78 Hu et al., 2009; Klapmeyer et al., 2012; Hsu et al., 2012a;b). For example, Hsu et al. (2013) and
79 Stafoggia et al. (2016) detected substantial increases of total particle number concentration (PNC) at
80 the airports of Los Angeles (CA, USA) and Rome Ciampino (Italy), respectively, in the few

81 minutes after take-offs, especially downwind, while landings made only a modest contribution to
82 ground-level PNC observations. Hsu et al. (2014) observed that departures and arrivals on a major
83 runway of Green International Airport (Warwick, RI, USA) had a significant influence on UFP
84 concentrations in a neighborhood proximate to the end of the runway. In a study carried out at the
85 Los Angeles international airport (CA, USA), Hudda et al. (2014) concluded that emissions from
86 the airport increase PNC by 4- to 5-fold at 8–10 km downwind of the airfield, while
87 Shirmohammadi et al. (2017) reported that the daily contributions of the airport to PNC were
88 approximately 11 times greater than those from three surrounding freeways. Hudda et al. (2016)
89 reported that average PNC were 2- and 1.33-fold higher at sites 4 and 7.3 km from the Boston (MA,
90 USA) airport when winds were from the direction of the airfield compared to other directions.
91
92 Despite the strong evidence that airports are major sources of UFPs, their fingerprint within the
93 particle number size distribution (PNSD) may be difficult to identify due to: (i) the nature of semi-
94 volatile compounds emitted by aircraft; (ii) the possible mechanisms of secondary aerosol
95 formation; (iii) the dilution effect; and (iv) the similar modal structures of other emission sources
96 concurrently found in cities, such as road traffic (Masiol and Harrison, 2014). Generally, studies
97 performed within or close to airports have reported increases of particles ranging from 4 to 100 nm
98 in diameter and mostly distributed in the nucleation range (<30 nm). For example, Mazaheri et al.
99 (2009) showed a main nucleation mode and an accumulation mode (40–100 nm) more evident
100 during take-offs; Keuken et al. (2015) reported PNSD dominated by 10–20 nm particles in an area
101 affected by emissions from Schiphol airport (The Netherlands); Hudda and Fruin (2016) found
102 strong increases in particles smaller than 40 nm downwind from the Los Angeles International
103 Airport; Ren et al. (2016) showed that particles peaking at 16 nm dominate the PNSD at various
104 distances from the runway of Tianjin International Airport, China; Masiol et al. (2016) reported that
105 the fingerprint of aircraft emissions sampled under real ambient conditions at the airport of Venice
106 (Italy) has a main mode at approx. 80 nm and a second mode in the nucleation range below 14 nm.

107

108 The Greater London area is home to more than 8.5 million inhabitants and is one of the few UK
109 locations not fully achieving the EU and national air quality standards: in 2015 nitrogen dioxide
110 breached the hourly and annual limit values for health, while ozone exceeded the long-term
111 objective (DEFRA, 2016). However, the standards were fully met for both PM₁₀ and PM_{2.5}.

112

113 London Heathrow (LHR) is one of the world's busiest international airports: it is ranked 1st in
114 Europe for total passenger traffic (ACI, 2016). It accommodates more than 1250 flights every day
115 and serves a total of 72.3 million passengers year⁻¹. LHR is composed of 5 terminals and 2 runways:
116 northern (3.9 km-long) and southern (3.7 km). Currently, runways operate near their maximum
117 capacity, with a consequent increase in the potential for delays when flights are disrupted. Since
118 2007, the proposal for expanding LHR with a 3rd runway and a 6th terminal has been intensely
119 debated in the UK. In 2016 the UK government provisionally approved the construction of a third
120 runway (UK Department for Transport, 2017).

121

122 LHR is located west of London (Figure SI1). Consequently, air quality in the surroundings of the
123 airport may be affected by the advection of air masses from the city, with the associated high levels
124 of pollutants emitted from traffic, energy demand for domestic heating and local industries. Airport
125 activities may also contribute to air pollution advected to the city when LHR is upwind, with
126 consequent potential impacts upon public health. In addition, as LHR attracts a large number of
127 passengers and workers, the emissions from large volumes of road traffic generated by the airport
128 and the nearby M4 and M25 motorways are difficult to discriminate from non-airport-related road
129 traffic. Due to this complex scenario, the contribution of LHR is difficult to differentiate from the
130 urban background pollution, as already reported by previous modelling and experimental studies
131 (Farias and ApSimon, 2006; Masiol and Harrison, 2015).

132

133 Various studies have attempted to quantify the effect of LHR upon air quality, mainly focusing on
134 the nitrogen oxides ($\text{NO}_x = \text{NO} + \text{NO}_2$), which are well-known tracers for aircraft engine exhausts
135 (e.g., Herndon et al., 2008; Masiol and Harrison, 2014 and references therein), but also arise from
136 other combustion sources. For example, Carslaw et al. (2006) estimated that airport operations in
137 2001/4 accounted for ~27% of the annual mean NO_x and NO_2 at the airfield boundary and less than
138 15% ($<10 \mu\text{g m}^{-3}$) at background locations 2-3 km downwind of the airport. Similar results were
139 found for the 2008/9 period using model evaluation (AEA, 2010) and for the 2005/12 period using
140 experimental data analysis (Masiol and Harrison, 2015). This latter study also reported that PM
141 mass concentrations at eight sites all around LHR were always well below the EU and UK limit.

142
143 This study aims to investigate the impacts of a major airport (LHR) serving a megacity (London)
144 upon the levels of submicrometre particles and to apportion those impacts to aircraft, road traffic
145 and other sources typical of large cities with airports. The main particle size distributions modes are
146 simplified by applying cluster analysis; then, the modal structures of the main potential sources are
147 disaggregated and the submicron particle number concentrations (PNC) are quantified through the
148 positive matrix factorisation (PMF). In addition, the origin of the airport plumes was spatially
149 assessed by matching results with local meteorological data, air mass movements, levels of
150 common air pollutants, $\text{PM}_{2.5}$ mass concentration and its chemical speciation as indicators of source
151 location and formation mechanisms.

152
153 The atmospheric chemistry and physical properties of UFPs have been extensively investigated in
154 London (e.g., Harrison et al., 2012; Jones et al., 2012; von Bismarck-Osten et al., 2013) with
155 several studies using cluster analysis (Beddows et al., 2009; Brines et al., 2014; 2015) or PMF
156 (Beddows et al., 2015; Vu et al., 2016). However, this study is the first one carried out in South-
157 West London to characterise and quantitatively apportion the impacts of LHR under real ambient
158 conditions. Moreover, only one earlier study (Masiol et al., 2016) has used both cluster analysis and

159 PMF to directly assess the airport contributions to UFPs. In addition, this study also investigated the
160 effects of a regional nucleation event on the results of the two source apportionment methods.

161

162 **2. MATERIALS AND METHODS**

163 **2.1 Experimental**

164 Two sampling campaigns (each 1 month-long) were carried out during warm (August-September
165 2014) and cold (December 2014-January 2015) periods at Harlington (Figure SI1). The site was
166 selected as well located to sample the plumes from the airport emissions: it lies 1.2 km N of the
167 northern runway and is located inside a playground, close to a secondary road and near the village
168 of Harlington. This is the location selected for the construction of the 3rd runway. The site is
169 categorised as “urban industrial” by DEFRA and it is therefore more indicative of community
170 exposure rather than direct fresh aircraft emissions. Consequently, it is a good point to quantify the
171 particles generated by the airport after a relatively short ageing and dispersion in the atmosphere,
172 and is more indicative of the fingerprint of aircraft emissions affecting communities than data
173 collected alongside the runway or in the airport apron areas. In addition, previous studies have
174 reported that the site is strongly affected by the plume from the airport (Carslaw et al., 2006; Masiol
175 and Harrison, 2015). Prevailing winds from the 3rd and 4th quadrants are recorded in both summer
176 and winter (Figure SI2): under such circulation regimes, Harlington lies just downwind of LHR.
177 The site is also affected by pollutants arising from the large volumes of road traffic within London,
178 from the local road network as well as those generated by the airport. Tunnel Rd., the main access
179 to LHR from the M4 motorway lies 800 m west, as well as the nearby M4 (640 m north) and M25
180 (~3.5 km east) motorways, major roads (Bath Rd, part of A4, passes 900 m south; A30 lies 2.8 km
181 SE). The village of Harlington (~400 m west) and advection of air masses from the conurbation of
182 London are other potential external sources.

183

184 Ultrafine particle counts and their size distributions from 14.3 to 673.2 nm were measured at 5 min
185 time resolution using a SMPS (scanning mobility particle sizer spectrometer) comprising an
186 electrostatic classifier TSI 3080 with a long differential mobility analyser (TSI 3081) and a CPC
187 (condensation particle counter, TSI 3775) based on condensation of *n*-butyl alcohol (Fisher
188 Scientific, ACS). The SMPS operated at a sheath air to aerosol flow ratio of 10:1 (sheath and
189 sample air flow rates were 3.0 and 0.3 L min⁻¹ respectively, voltage 10-9591 V; density 1.2 g/cc;
190 scan time 120 s, retrace 15 s; number of scan 2) while the CPC operated at low flow rate (0.3 L
191 min⁻¹). The use of 5 min resolved spectra has already been used successfully for source
192 apportionment purposes at an airport (Masiol et al., 2016).

193
194 Equivalent Black Carbon (eBC) as defined by Petzold et al. (2013) was also measured at 5 min
195 resolution using a 7-wavelength aethalometer (Magee Scientific AE31). The aethalometer operated
196 with an inlet cut-off head to collect PM with aerodynamic diameter of <2.5 µm (PM_{2.5}). eBC was
197 derived from the absorbance at 880 nm wavelength (Petzold et al., 2013); raw data were post-
198 processed with the Washington University Air Quality Lab AethDataMasher V7.1 to perform data
199 validation and correct data for non-linear loading effects (Virkkula et al., 2007; Turner et al., 2007).

200
201 Instruments were installed into a plastic/metal case designed for sampling purposes: (i) air inlets
202 were ~1.8 m above the ground and were composed of conductive materials to avoid particle losses
203 and sampling artefacts; (ii) the case was cooled by fans in summer and was warmed by an electrical
204 tubular heater in winter for maintaining an indoor air temperature within an acceptable range for
205 running the equipment (temperature inside the case was recorded and periodically checked); (iii)
206 instruments were isolated from vibration using rubber pads and foam foils. Devices were fully
207 serviced, calibrated by authorised companies and underwent internal cross-calibrations with other
208 similar instruments under lab conditions. Moreover, frequent periodic checks, maintenance of
209 instruments and cleaning of inlets was performed throughout the sampling campaign.

210

211 Routine air pollutants (NO, NO₂, NO_x, O₃, PM₁₀, PM_{2.5}) were measured at Harlington with 1 h time
212 resolution by the UK Automatic Urban and Rural Network under the auspices of the UK
213 Department for Environment, Food and Rural Affairs (DEFRA; <http://uk-air.defra.gov.uk/>).
214 Gaseous species were analysed using automatic instruments according to European standards and
215 National protocols: EN 14211:2012 for nitrogen oxides and EN 14625:2012 for ozone. PM₁₀ and
216 PM_{2.5} were analysed using tapered element oscillating microbalance and filter dynamics
217 measurement system (TEOM-FDMS) to provide measurements accounting for volatile (VPM₁₀,
218 VPM_{2.5}) and non-volatile (NVPM₁₀, NVPM_{2.5}) fractions. Quality assurance and quality control
219 procedures followed the standards applied for the Automatic Urban and Rural Network (AURN)
220 and the London Air Quality Network (LAQN). Instruments were routinely calibrated, and every six
221 months were fully serviced and underwent intercalibration audits.

222

223 Some additional variables are also computed from the air pollutants to help the interpretation of
224 results. The NO₂/NO_x ratio is indicative of the partitioning of nitrogen oxides, while the levels of
225 oxidants (OX=O₃+NO₂, expressed in ppbv) can be used to roughly assess the oxidative potential in
226 the atmosphere (Kley et al., 1999; Clapp and Jenkin, 2001). These two new variables are useful in
227 investigating the atmospheric chemistry behind the NO-NO₂-O₃ system. Delta-C (the difference
228 between absorbance at 378 and 880 nm, also called UVPM) was also computed. This variable was
229 largely used as a proxy to estimate the fraction of carbonaceous material emitted by biomass
230 burning (e.g., Sandradewi et al., 2008; Wang et al., 2011). However, Delta-C results should be used
231 with caution: Harrison et al. (2013) showed that there are probably other UV absorbing contributors
232 than wood-smoke to the aethalometer signal. Consequently, Delta-C is used here only for
233 qualitative purposes.

234

235 Weather data were measured hourly by the Met Office at LHR; met data include wind direction and
236 speed, atmospheric pressure, air temperature, relative humidity (RH), visibility, rain and solar
237 irradiance.

238

239 During the two campaigns, 24-h PM_{2.5} samples were also collected on quartz filters using a high
240 volume air sampler (TE-6070, Tisch Environmental, Inc.) and analysed for the daily concentrations
241 of major PM_{2.5} components: organic carbon (OC) and elemental carbon (EC) by thermo-optical
242 analysis (EUSAAR_2 protocol) and major inorganic ions (Na⁺, K⁺, ammonium, nitrate, sulphate,
243 oxalate) by ion chromatography. Analytical methods are reported in detail in Yin et al. (2010). The
244 results of the chemical speciation of PM_{2.5} are presented in a companion paper (in preparation) and
245 are used in this study only to assist the interpretation of PMF results.

246

247 **2.2 Data Handling and Chemometric Approaches**

248 Data were analysed using R version 3.3.1 (R Core Team, 2015) and a series of supplementary
249 packages, including ‘Openair’ (Carslaw and Ropkins, 2012). Preliminary data handling and clean-
250 up were carried out to check the robustness of the dataset, detect anomalous records and to delete
251 extreme outliers. SMPS data with unreliable behaviour or instrument errors were completely
252 deleted. An in-depth analysis of the dataset revealed few records with anomalously high PNC,
253 which were likely related to probable instrumental issues, extreme weather conditions (e.g., high
254 wind gusts, heavy rain striking the inlet), or infrequent local emissions, e.g., maintenance, painting
255 and recreational activities (including fires) on the playground where the site is located, road
256 maintenance close the site and probable short-term parking of high-emission vehicles near the site.
257 Since this study aims to investigate the overall contributions of LHR, all data are used for
258 descriptive statistics, but data greater than the 99.5th percentile were further removed for
259 explorative, cluster and PMF analyses. This data exclusion successfully removed the extremely high
260 events occurring during the sampling campaigns and significantly improved the stability and

physical meaning of PMF solutions. Missing data for other variables were linearly interpolated between the nearest values of the time series.

The particle number size distributions (PNSDs) were firstly grouped by applying a k -means cluster analysis. The full method is exhaustively discussed in Beddows et al. (2009; 2014) and aims to assemble single spectra into k clusters. The clustering groups observations with spectra similar to their cluster centroids (means), i.e. observations that are likely generated by the same set of formation processes or emission sources. The optimum number of clusters (k) was determined by an optimisation algorithm based on the spectral shapes (Beddows et al., 2009). The choice to apply the k -mean clustering method was based on several reasons: (i) Salimi et al. (2014) reported that k -means is the best performing clustering among others methods tested on PNSD data; (ii) k -means is a well-established method which has been widely applied over a number of different sites (e.g., Dall'Osto et al., 2012; Wegner et al., 2012; Beddows et al., 2014; Brines et al., 2014; 2015); and (iii) the method was previously applied successfully to airport data (Masiol et al., 2016).

PMF analysis was performed by applying the USEPA PMF5 model. Details of the PMF model are reported elsewhere (Paatero and Tapper, 1994; Paatero, 1997; USEPA, 2014), while the best practice and standards are extensively reviewed in several papers (e.g., Reff et al., 2007; Belis et al., 2014; Brown et al., 2015; Hopke, 2016). SMPS data at 5 min resolution were used as the PMF input matrix. Uncertainties associated with SMPS data were estimated according to the empirical method proposed by Ogulei et al. (2007). Uncertainty for the total variable (total particle number concentration, PNC) was set at 300% of the PNC concentration and also marked as “weak” to avoid it driving the profiles.

The best PMF solutions were identified: (i) by investigating solutions between 3 and 10 factors; (ii) by considering the minimization of the objective function Q with respect to the expected (theoretical) value and its stability over multiple ($n=100$) runs, (iii) by obtaining low values for the

287 sum of the squares of the differences in scaled residuals for each base run pair by species; (iv) by
288 minimizing the number of absolute scaled residuals over ± 3 and by keeping them symmetrically
289 distributed; (v) by keeping the result uncertainties calculated by bootstrap (BS, $n=200$) and
290 displacement (DISP) methods within an acceptable range (Paatero et al., 2014); (vi) by obtaining
291 modelled total variable (PNC) successfully predicted ($R^2 > 0.9$ and slopes ≈ 1); and (vii) by avoiding
292 the presence of edges in the G-space plots (Paatero et al., 2002) and, then, the presence of
293 hidden/unresolved sources.

294
295 A series of additional tools were used to analyse the raw data, link source apportionment results to
296 other variables, such as local atmospheric circulation and regional/transboundary transport of air
297 masses. Briefly, polar plots aim to map pollutant average concentrations by wind speed and
298 direction as continuous surfaces (Carslaw et al., 2006), while polar annuli plot by wind direction
299 and hours of the day. The potential locations of distant sources were assessed using back-trajectory
300 analysis and a concentration weighted trajectory (CWT) model (Stohl, 1998). Back-trajectories
301 were computed with the HYSPLIT4 model (Stein et al., 2015; Rolph, 2016) using NCEP/NCAR
302 reanalysis gridded meteorological data. Set-up: -96 h with a starting height of 500 m a.g.l. CWT is a
303 method of weighting trajectories with associated concentrations to detect the most probable source
304 areas of long-range transports of pollutants; it has been used and reviewed in a number of prior
305 studies (e.g., Stohl, 1996; Lupu and Maenhaut, 2002; Squizzato and Masiol, 2015).

310 **3. RESULTS AND DISCUSSION**

311 **3.1 Overview of Data**

312 The wind roses during the two sampling periods are provided in Figure SI2. Descriptive statistics of
313 all collected variables are reported as boxplots in Figure SI3. PNSDs were initially split into 3
314 ranges: nucleation (14-30 nm), Aitken nuclei (30-100 nm) and accumulation (>100 nm). On
315 average the total PNC during the warm season was 1.9×10^4 particles cm^{-3} , of which 1.1×10^4 , $6.4 \times$
316 10^3 and 1.5×10^3 particles cm^{-3} were classified as nucleation, Aitken and accumulation ranges,
317 respectively (Figure SI3). During the cold season, the total average PNC was 2.2×10^4 particles
318 cm^{-3} , composed of 1.4×10^4 , 6.3×10^3 and 1.4×10^3 particles cm^{-3} as nucleation, Aitken and
319 accumulation ranges, respectively (Figure SI3). Concentrations lie between those of London,
320 Marylebone Road (kerbside) and London, North Kensington (background), and nucleation particles
321 were ~10 times higher than the annual average measured in North Kensington as reported by Vu et
322 al. (2016), while Aitken particles were 1.9 times higher. It is therefore evident that the main
323 difference lies in the concentration of the finest size ranges: in both seasons, spectra were
324 dominated by UFP ($D_p < 100$ nm) particles (~92% of total PNC), which only accounted for ~12% of
325 total particle volume concentration (PVC, computed by approximation to spherical particles). On
326 the other hand, accumulation mode particles accounted for ~8% of PNC and ~88% of PVC volume.
327 The high levels of total PNC are not surprising: several studies carried out into or close to airports
328 (e.g., Hsu et al., 2013;2014; Hidda et al., 2014; 2016; Stafoggia et al., 2016; Shirmohammadi et al.,
329 2017) reported significant increases in the concentrations of UFPs.

330

331 During the two sampling campaigns, air pollutants measured in Harlington (Figure SI3) were
332 similar to the average concentrations measured over an 8 year period (2005-2012) in the vicinity of
333 LHR (Masiol and Harrison, 2015). Consequently, despite the two short campaigns carried out in
334 this study, results may be considered representative of the average levels of air pollution recorded at
335 Harlington. The average concentrations of eBC were 2.4 and $2.1 \mu\text{g m}^{-3}$ during the warm and cold
336 season, respectively. The average concentration of Delta-C was $0.1 \mu\text{g m}^{-3}$ during the warm season
337 and $0.36 \mu\text{g m}^{-3}$ in winter.

338

339 Analysis of the data showed a non-normal distribution for most of the variables: the nonparametric
340 Kruskal-Wallis one-way analysis of variance was therefore used to test the difference of
341 concentrations over the two periods (Kruskal and Wallis, 1952): almost all variables are different at
342 the 0.05 significance level, except NO, NO_x and O₃. This result indicates a seasonal effect upon air
343 quality in the LHR area and suggests investigating the sources over the two periods separately.

344

345 The average PNSDs are shown in Figure 1 as well as their median distributions and interquartile
346 ranges. Spectra are categorised by time of day (7am-7pm and 7pm- 7am local time). In addition, the
347 particle volume size distributions (PVSDs) are also provided. Results for the warm season show
348 that the average daytime PNSD is dominated by a main peak in the nucleation range (extending
349 below 14 nm) and a second mode in the Aitken range (between 30 and 50 nm). The nocturnal
350 spectrum is characterised by a drop of the nucleation mode to concentration values similar to the
351 Aitken peak (mode around 35 nm). During the cold season, the average diurnal and nocturnal
352 PNSDs present a main peak at 15-25 nm and a second mode at 70-100 nm. In summary, both
353 seasons show reductions of the finest modes during nighttime, while the second mode is almost
354 constant throughout the day. As a consequence, the modal structure of PNVDs is also almost
355 constant throughout the day.

356

357 The diurnal cycles of the 3 particle ranges, eBC, solar irradiation and airport movements are shown
358 in Figure 2. A comprehensive overview of the patterns for all the variables is provided in Figure
359 SI4. Generally, diurnal cycles derive from the interplay of emissions, dispersion and atmospheric
360 chemical processes. Consequently, they need to be investigated along with patterns for airport and
361 motorway traffic (Figure 2 and Figure SI5, respectively), and as polar annuli (Figures SI6 and SI7)
362 and polar plots (Figures SI8 and SI9), which give preliminary insights into the origin and spatial
363 location of most probable emission sources. During nighttime, airport traffic is restricted to limit

364 noise and community disturbance: flights are generally constant from 6 am to 8 pm and are kept at
365 minimum overnight, with no departures normally scheduled between 11 pm and 6 am (Figure 2).
366 Road traffic is more difficult to define. Data for M4 and M25 motorways are provided by the UK
367 Department for Transport: data for the M4 motorway show typical morning (7-8 am) and evening
368 (5-6 pm) peaks due to rush hours, but this pattern is not well-resolved for the M25 (Figure SI5). In
369 addition, despite it being likely that traffic on minor and local roads also follows patterns dominated
370 by rush hours, traffic generated by the airport is more difficult to characterise, with Tunnel Rd. and
371 other busy roads serving LHR being frequently congested.

372

373 Nucleation particles are likely associated with aircraft movements. The daily pattern shows high
374 and almost constant concentrations between 7 am and 11 pm (Figure 2): hourly averages ranged
375 from 10×10^3 to 15×10^3 particles cm^{-3} during the warm season and from 10×10^3 to 21×10^3
376 particles cm^{-3} during the cold season. On the contrary, the concentrations of nucleation particles
377 significantly (Kruskal-Wallis at $p < 0.05$) drop overnight (hourly averages ranging from 5×10^3 to
378 $6 \cdot 10^3$ particles cm^{-3} and from 1×10^3 to $5 \cdot 10^3$ particles cm^{-3} during the warm and cold season,
379 respectively); the maximum average concentrations are recorded for winds blowing from the SW
380 quadrant (polar plots and polar annuli in Figures SI6-9), i.e. the airfield and, in particular, the
381 location of the main LHR terminals (Figure SI1). As a consequence of the dominance of nucleation
382 particles over size spectra, also total PNC follows the pattern (Figures 2) and wind directionality
383 (Figures SI8-9) of nucleation particles. On the contrary, accumulation particles appear to be more
384 associated with road traffic. These particles increase for winds blowing from northern sectors
385 (Figures SI6-9), i.e. toward the M4. Accumulation particles also present the morning (6-8 am) and
386 evening (6-11 pm) rush hour peaks during the warm season, but only the evening peak (from 6 pm
387 to the night) was found in the cold season (Figure 2). Generally, the evening peaks start around 6
388 pm, which is consistent with the peak of traffic (Figure SI5) but they extend late in the evening and
389 night probably because the drop of the mixing layer top and the consequent concentration of

390 pollutants close to the ground level. Aitken nuclei exhibit a mixed behaviour between nucleation
391 and accumulation particles (Figure 2): two different patterns can be found, which are more
392 consistent with road traffic in summer and with aircraft traffic in winter.

393

394 Despite some studies indicating that airports are strong sources of black carbon (Dodson et al.,
395 2009), other studies report no strong relationships with the flight activity (Masiol et al., 2016; Hsu
396 et al., 2016). Similarly to NO₂ (Figure SI4) and accumulation particles (Figure 2), aethalometer data
397 also shows typical patterns of road traffic-influenced sites for all wavelengths, with two daily peaks
398 corresponding to the hours with higher traffic (Figure 2). However, Delta-C does not present any
399 evident pattern (Figure SI4). eBC shows increased concentrations when winds blow from northern
400 sectors (plus SE in winter, Figure SI7 and SI9); which excludes airport activities as being a
401 dominant source in the study area.

402

403 Particulate matter mass concentration (PM₁₀ and PM_{2.5}) has very weak diurnal patterns (Figure SI4).
404 Its wind directionality shows evident increases for northerly winds (Figure SI8-9). It is therefore
405 evident that PM mass concentrations are dominated by non-airport sources, i.e. regional secondary
406 pollutants, traffic from the nearby M4 or background pollution from London. PM_{2.5} concentrations
407 normally do not exceed the Limit Values in the Greater London area (DEFRA, 2016).

408

409 **3.2 *k*-means Cluster Analysis**

410 The clustering algorithm extracted 5 clusters for both periods. The number of clusters was selected
411 according to the optimisation algorithm, i.e. local maxima in the Dunn indices and silhouette
412 (Beddows et al., 2009). The extraction of 5 clusters represents a good compromise for the
413 interpretation of spectral observations. Hussein et al. (2014) reported that is not prudent to describe
414 the spectra with few clusters (2-4), which are not sufficient to explain variations and detailed

415 differences in the PNSD observed in the urban atmosphere. On the other hand, they also reported
416 that extracting too many (>10) clusters may make the aerosol source attribution more challenging.
417

418 The cluster centroids (mean spectra of each cluster), the 10th, 25th, 75th and 90th percentile, the
419 hourly counts patterns and resulting wind roses are shown in Figures 3 and 4 for the warm and cold
420 season campaigns, respectively. Despite extracted clusters exhibiting significantly different modal
421 structures for PNC, no differences can be observed for the particle volume size spectra, which all
422 show a unimodal peak at approx. 200-300 nm. Clusters accounted for 14%-25% of total
423 observations for both the seasons: Table SI1 summarises the percentage of the total observations for
424 each cluster.

425

426 Three clusters (*cluster 1* during the warm season and *clusters 1 and 5* in winter) are likely shaped
427 by the airport emissions. The modal structures present sharp peaks for nucleation particles which
428 extend below the SMPS detection limit (14 nm) and drop at 30-40 nm; no secondary modes are
429 present in the Aitken or accumulation ranges. These clusters show a large increase in frequency
430 during the afternoon and evening hours (cluster 1 for the warm season and cluster 5 for the cold
431 season) or extended over the daytime (cluster 1 for the cold season), similarly to the airport aircraft
432 movement profiles (Figure 2). Aircraft are known to emit particles in the nucleation range (e.g.
433 Mazaheri et al., 2009;2013; Masiol and Harrison, 2014; and references therein; Lobo et al., 2015)
434 and the wind roses are also compatible with an origin from the airfield and the main LHR terminals
435 (Figures 3 and 4). However, daytime regional photochemical nucleation events in London occur
436 around noon-2 pm and are mostly recorded from June to September (Vu et al., 2016).

437 Consequently, the modal structure of cluster 1 for the warm season could be additionally shaped by
438 regional photochemical nucleation. The reasons driving the split of the spectra likely shaped by
439 LHR into two clusters during the cold season are unclear. A further comparison of the cluster and
440 PMF results will help in interpreting this outcome.

441

442 The modal structures of the *clusters 4* for both seasons peak for nucleation particles and extend
443 below 14 nm, but also show probable modes between 50 and 200 nm (Figures 3 and 4). They
444 represent the typical spectra associated with aged anthropogenic emissions, mostly due to road
445 traffic. It is recognised that road traffic contributes to a large range (30-200 nm) of PNSD in the
446 urban atmosphere (e.g., Yue et al., 2008; Costabile et al., 2009; Harrison et al., 2011), which is
447 compatible with these spectra. The directional analysis for the warm season shows increased levels
448 when air masses move from the sectors more affected by traffic, i.e. London (NE), M4 (N) and M25
449 (W) motorways and Tunnel Rd (W), while the hour count profile presents a huge maximum during
450 daytime. In winter, this modal structure mostly occurred for westerly winds: the atmospheric
451 circulation during the cold season mostly experienced winds blowing from the SW quadrant, with
452 NE sectors poorly represented (Figure SI1). As a consequence, the limited number of observations
453 for air pollution advected from the Greater London area may have affected the detection of the
454 urban background from London. This lack of data is also reflected by diurnal profile, which shows a
455 marked peak in the late afternoon, concurrent to the peak of traffic on M4 and M25 (Figure SI5).

456

457 Three clusters (*clusters 2* and *3* during the warm season and *cluster 2* in winter) exhibited similar
458 hourly profiles with most of the counts occurring overnight (Figures 3 and 4). This pattern is largely
459 attributable to the dynamics of the mixing layer, since the diurnal cycles are the mirror image of the
460 ambient air temperature (Figure SI4). Because of this, these clusters could be potentially affected by
461 the reduced height of the mixing layer occurring overnight. These clusters exhibit bimodal
462 structures with the coarser modes with respect to the remaining clusters: cluster 2 for the warm
463 season shows a main peak in number concentrations at 30-40 nm and a second peak in the finest
464 range (<16 nm), clusters 3 for the warm season peaks at 14 and 60-70 nm, and cluster 2 for the cold
465 season extends over a wide size range with two modes around 20-30 nm and 100-150 nm.

466 Consequently, these clusters are likely representative of spectra mostly shaped by the drop of the

467 mixing layer height and the formation of secondary aerosols. In this context, the potential role of
468 nighttime nitrate formation through condensation of NH_4NO_3 and the heterogeneous reactions of
469 N_2O_5 and NO_3 on pre-existing particles cannot be ignored (Seinfeld and Pandis, 2006; Bertram and
470 Thornton, 2009; Brown and Stutz, 2012). The wind roses reveal that both clusters 2 occur under
471 similar westerly wind regimes. Regional aerosols appear to be the most probable source. On the
472 contrary, cluster 3 for the warm season occurs with winds from London (NE) and likely represents
473 particle size spectra mainly shaped by primary and secondary aerosols advected from the most
474 urbanised areas, i.e. it is most likely associated with the urban background of London.

475

476 *Cluster 5* for the warm season and *cluster 3* for the cold season may be associated with road traffic.
477 They reveal modal structures with a dominant peak around 20-35 nm (cluster 5 also shows a
478 possible second peak at 15 nm) and mostly occur when air masses blow from westerly sectors,
479 which are compatible with the location of motorways and Tunnel Rd, the main roadway linking
480 LHR to the M4 motorway. In summer, the hourly count pattern exhibits two maxima (6-8 am and 4-
481 8 pm) related to morning and evening rush hours; this pattern is compatible with fresh road traffic
482 emissions. However, the diurnal pattern in winter also presents a high number of counts at 3-5 am,
483 i.e. not directly compatible with rush hours. A possible explanation involves the stronger effect of
484 the winter mixing layer dynamics on the air quality due to the presence of more frequent low level
485 thermal inversions, which may build up the pollutants at ground-level especially overnight. This
486 may increase the signal of the less intense, but still significant, nighttime traffic emissions present in
487 the study area.

488

489

490

491 **3.3 PMF Analysis**

492 The interpretation of PMF results was then attempted by considering: (i) the knowledge of sources
493 impacting the study area; (ii) the comparison with the results reported by Vu et al. (2016), who
494 performed a PMF analysis of SMPS data collected in North Kensington (London urban
495 background); (iii) the shape of resulting profiles for both the particle number and volume
496 concentrations; (iv) the analysis of diurnal patterns; (v) the directional analysis using the polar plot
497 and polar annuli; (vi) the correlations between the source contributions and the other air pollutants
498 monitored at the site or with weather variables, and (vii) the analysis of possible remote source
499 areas by applying the CWT model.

500

501 Six-factor solutions were extracted for both the seasons. The resulting factor profiles are presented
502 in Figures 5 and 6 for the warm and cold season, respectively. The factor profiles are expressed as:
503 (i) particle number concentrations and their DISP ranges; (ii) particle volume concentrations, and
504 (iii) explained variations showing how much of the variance (from 0 to 1) in the original dataset is
505 accounted for by each extracted factor. The Figures 5 and 6 also show the diurnal patterns and the
506 polar plots computed from the hourly-averaged contributions. Table 1 summarises the PMF results
507 and spectral characteristics, while Table 2 shows the Pearson correlation matrices with weather and
508 air quality variables. Selected PMF solutions were very stable: no errors or unmapped factors and
509 few swaps (none in summer and $<7\%$ in winter) were found in BS; no swaps or errors even at
510 $dQ_{max}=25$ were found for DISP, i.e. solutions were affected by small rotational ambiguity and,
511 therefore, their interpretation can be considered robust.

512

513 DISP analysis is designed to explore the realistic bounds on the optimal (base run) PMF solutions
514 that do not result in appreciable increases in the Q values (Brown et al., 2015). In this study, the
515 ranges calculated by DISP for the $dQ=4$ were used to assess the uncertainty boundaries associated
516 with the final PMF profiles, as suggested in Zikova et al. (2016) and Masiol et al. (2017). This

strategy is useful to better interpret the results, as the regions of spectra affected by high rotational ambiguity are disclosed in the resulting profiles.

3.3.1 Warm season

Factor 1 includes most of the particles in the nucleation range (<20 nm), exhibits a sharp mode in the number distribution below the SMPS detection limit (14 nm) and makes the largest contribution to the total PNC (31.6%, DISP range 31-36%) (Figure 5). However, its contribution to the volume distribution is ~1%. Several studies report that particles in the nucleation range are emitted from aircraft engines (e.g., Anderson et al., 2005; Herndon et al., 2008; Kinsey et al., 2010; Mazaheri et al., 2009;2013; Masiol and Harrison, 2014; Lobo et al., 2015) as well as from other anthropogenic (e.g., Schneider et al., 2005; Chen et al., 2011; Cheung et al., 2012; Stevens et al., 2012; Kumar et al., 2013;2014; Vu et al., 2015b) and natural (e.g., Kulmala et al., 1998; O'Dowd et al., 1998;1999; Kulmala and Kerminen, 2008; Riccobono et al., 2014) sources. This factor does not show any significant ($p < 0.05$) and strong ($r \geq |0.6|$) correlation with other measured species, but shows a weak ($|0.4| \leq r < |0.6|$) correlation with Factor 2 (Table 2). Its diurnal variation (Figure 5) shows higher concentrations between 6 am and 10 pm, and well agrees with the airport flight movements (Figure 2). The polar plot analysis also indicates enhanced levels when winds $> 2 \text{ m s}^{-1}$ blow from the airfield sectors (SW). All these insights are consistent with the location of Heathrow, i.e. the most plausible interpretation is related to the aircraft engine exhaust emissions. This interpretation is also supported by Keuken et al. (2015), which shows that the PNSD in an area affected by emissions from Schiphol airport (The Netherlands) is dominated by ultrafine (10-20 nm) particles. The large contribution of this factor to the total PNC is not surprising if compared to the results reported for the Los Angeles international airport by Hudda et al. (2014) (emissions from the airport increased PNC 4- to 5-fold at 8–10 km downwind the airfield). Since the airport of Los Angeles and LHR have comparable aircraft traffic, the quite high concentrations found in this study (on annual average nucleation particles are ~10 times higher than those measured in North Kensington urban

background by Vu et al. (2016)) are consistent with the sampling location chosen in this study (~1.2 km to the airfield). In addition, this result also agrees with previous studies on the impacts of LHR on local air quality; Carslaw et al. (2006) and Masiol and Harrison (2015) found comparable percent contributions of LHR emissions on NO₂ levels in the study area (approx. 25-30%). However, the lack of correlations with NO and NO₂ (tracers for aircraft emissions) is probably due to the presence of several other sources of nitrogen oxides in the area, such as the heavy traffic generated from the airport and from the nearby motorways.

Factor 2 is made up of ultrafine particles in the nucleation-Aitken range (one main peak at 20-35 nm) and accounts for 28% (DISP 25-30%) of PNC; its contribution to the volume distribution is low (~2%) and peaks at 22-45 nm and at 140-220 nm (Figure 5; Table 1). Several insights seem to link this factor to road traffic emissions: (i) the modal structure; (ii) the strong association with morning and evening rush hours, and (iii) the significant increase for winds in the west and south-westerly sectors consistent with emissions generated from local busy roads close to LHR, Tunnel Rd. and M25 motorway. A similar mode in the nucleation range has been extensively attributed to the size distribution from road traffic (e.g., Vogt et al., 2003; Zhang et al., 2004; Ntziachristos et al., 2007; Vu et al., 2015b) and the growth of nucleation particles from diesel vehicles (Mayer and Ristovski, 2007; Wehner et al., 2009). For example, Charron and Harrison (2003) reported that particles in the range 30–60 nm show a stronger association with light-duty traffic at a traffic hotspot in central London (Marylebone Rd.); Janhäll et al. (2004) reported an average particle size distribution peaking at 15-30 nm during morning peak high traffic intensity in the city of Göteborg (Sweden), which has a car fleet comparable to the UK; Ntziachristos et al. (2007) found a sharp mode at 20-30 nm in sampling from engine exhausts. In addition, PMF factors with similar modal structures were found in other studies and were attributed to road traffic emissions: among others, Harrison et al. (2011) linked a factor peaking at 20 nm to primary road traffic emissions near a major UK highway; Masiol et al. (2016) measured PNSD in an international airport in Northern

Italy during summer and interpreted a factor with a clear mode at 35–40 nm as road traffic from the nearby city; Beddows et al. (2015) and Vu et al. (2016) found traffic factors with modal diameter at around 30 nm in an urban background site in London (North Kensington); Sowlat et al. (2016) reported a factor peaking at 20–40 nm in number concentration and at around 30–40 nm in volume concentration in Los Angeles (US) and interpreted it as traffic tailpipe emissions. However, this factor lacks significant positive correlations with primary road traffic tracers (nitrogen oxides, eBC; Table 2), while other studies have reported weak positive correlations with such species (Harrison et al., 2011; Masiol et al., 2016; Vu et al., 2016; Sowlat et al., 2016). Similarly to factor 1, this latter result may be due to the difference in the time resolution between chemical species and PNSD and the presence of several sources of nitrogen oxides in the area.

Factor 3 is mostly represented by 25–90 nm particles and contributes about 19% (17–21%) to the total number concentration (Figure 5; Table 1). It also shows a second mode below the SMPS detection limit (14 nm), however, the DISP range clearly indicates that this part of the profile is affected by a large amount of rotational ambiguity, so that the presence of this second mode should be interpreted with caution. The volume concentration peaks at around 40–100 nm and 250–450 nm. The factor contribution is higher during rush hours, but the morning peak occurs 1 h later than in factor 2. The wind directionality shows increases for air masses blowing gently ($<4 \text{ m s}^{-1}$) from W and for calm wind periods, suggesting a quite local source; however, also an increase of concentrations is found for higher wind regimes ($>6 \text{ m s}^{-1}$) from the East (London). Factor 3 also shows significant positive correlations with NO (0.43) and NO₂ (0.61) (Table 2). All these insights seem to point to an aged road traffic source. This interpretation is also supported by Vu et al. (2016), who found a similar factor in London (North Kensington) peaking at ~20–100 nm. In this context, several source apportionment studies on PNSDs have attributed more than one factor to road traffic (e.g. Kasumba et al., 2009; Thimmaiah et al., 2009; Harrison et al., 2011; Liu et al., 2014; Al-Dabbous and Kumar, 2015; Vu et al., 2016; Sowlat et al., 2016). This result is not

surprising in areas where heavy traffic is widespread, as particles may undergo condensation, agglomeration, evaporation and dilution processes and, consequently, they may change modal characteristics in time and space. Such atmospheric processes are the main mechanisms reshaping PNSDs after primary exhaust is emitted into the atmosphere and have been discussed in several studies (Shi et al., 1999; Kim et al., 2004; Zhang et al., 2005; Zhou et al., 2005; Kulmala and Kerminen, 2008; Zhang et al., 2011; Harrison et al., 2016).

Factor 4 is made up of particles over a wide range (50-200 nm with a clear mode at ~80 nm for PNC and 60-300 nm for PVC). The factor contributes 14% of PNC, but accounts for the main percentage of the volume concentration (33%). This factor correlates well with gaseous pollutants linked to combustion sources (mostly road traffic), i.e. NO (0.6), NO₂ (0.76), and non-volatile primary pollutants, such as eBC (0.62), NVPM_{2.5} (0.62) and EC (0.75) (Table 2). The factor also strongly correlates with OC (0.84) and sulphate (0.75). The diurnal pattern shows two main peaks in the morning and evening rush hours (Figure 5), but the concentrations recorded between the two maxima are higher overnight than during daytime. This pattern suggests that both local emission sources and the dynamics of the mixing layer may play a key role in shaping its diurnal cycle, i.e. emitted pollutants undergo a wide dispersion within the expanded mixing layer during the daytime, while the drop of the mixing layer top occurring overnight restricts those pollutants to a layer close to ground level. The polar plot indicates increased levels for calm wind conditions or winds blowing from London (East sectors); in addition, the factor is strongly negatively correlated with wind speed (-0.64) (Table 2).

All these insights suggest that Factor 4 represents the fingerprint of the London pollution. Several studies carried out in London (Beddows et al., 2009;2015; Vu et al., 2016) and other megacities (e.g., New York: Masiol et al., 2017) have reported similar results, all interpreting this source profile as urban background (or urban accumulation mode). This source comprises both the solid

621 particle mode from traffic emissions (Harrison et al., 2011; Pant and Harrison, 2013; Dall'Osto et
622 al., 2012) and secondary species condensed upon pre-existing particles acting as condensation
623 nuclei, including secondary sulphate, nitrate and organic aerosols. Secondary sulphate is formed
624 through the atmospheric processing of local or distant SO₂ emissions (Kerminen et al., 2000) and
625 neutralisation with ammonia (Benson et al., 2011). Nitrate aerosol is formed through the oxidation
626 of NO₂ to nitrate and the consequent neutralization with ammonia (Seinfeld and Pandis, 2006) and
627 occurs during both daytime and night-time; however the semivolatile nature of ammonium nitrate,
628 makes its partitioning to the condensed-phase very weak. This behaviour also favours the
629 occurrence of negative artefacts in filter-based sampling, which may explain the lack of significant
630 correlations between the factor and the PM_{2.5}-bound nitrate (Table 2). On the contrary, the increase
631 of the intensity of factor 4 during the night-time and the significant association with NO₂ are highly
632 consistent with the chemistry driving the heterogeneous reactions of N₂O₅ and NO₃ on aerosol
633 surfaces (Bertram and Thornton, 2009; Brown and Stutz, 2012). In view of this, Dall'Osto et al.
634 (2009) reported that most nitrate particles in London are: (i) locally produced in urban locations
635 during nighttime; (ii) mainly present in particles smaller than 300 nm and (iii) internally mixed with
636 sulphate, ammonium, EC and OC.

637

638 Factors 5 and 6 make small contributions to PNC (4-7% and 1-4%, respectively), but are relevant
639 for the volume concentration (37% and 21%, respectively). Factor 5 shows a main accumulation
640 mode in number concentration at 110-250 nm and two more modes at ~30-70 nm and below 14 nm
641 (Figure 5; Table 1); however, the latter two modes suffer of large rotational ambiguity and should
642 be interpreted with care. On the contrary, it exhibits a wide mode in volume concentration ranging
643 from ~100 to ~500 nm. Factor 6 has two relevant modes in number concentration at 55-120 nm and
644 230-400 nm, and two modes in volume concentration at 260-500 nm and 75-140 nm.

645

646 These factors still present two peaks corresponding to the rush hours, but the morning peak occurs
647 1-2 h earlier than in the road traffic-related factors, i.e. when ambient temperature reaches its daily
648 minimum. Both factors correlate well with secondary aerosol tracers (nitrate, sulphate, OC) and
649 non-volatile components (eBC, EC, NVPM_{2.5}), but Factor 6 exhibits much higher correlation
650 coefficients (Table 2). Despite the polar plots indicating the main wind directionality toward N-E
651 sectors, the analysis of air mass histories through the CWT model (Figure 7) clearly indicates likely
652 continental origin areas rather than local sources.

653

654 Vu et al. (2016) observed two factors in North Kensington with very similar modal structures, daily
655 patterns, correlations with PM_{2.5}-bound species and external source areas maps. Therefore, their
656 interpretation is confirmed also in this study, i.e. mixed secondary aerosol (Factor 5) and inorganic
657 secondary aerosol (Factor 6). Both factors are clearly originated from continental Europe and are
658 consistent with a previous receptor modelling study carried out in a rural background site
659 representative of the southern UK (Charron et al., 2013). Similar origin and formation mechanisms
660 also explain their strong correlation (0.75). Although it is not reasonable to extract much more
661 information from these data due to the short period of sampling and the large uncertainty associated
662 with back-trajectory analysis, it can be observed that Factor 5 shows a wide source area all over
663 Central Europe, while Factor 6 exhibits two distinct hotspots (Central and North-eastern Europe).

664

665

666 3.3.2 Cold season

667 The 6 factors identified during the cold period (Figure 6) are similar to those for the warm season.
668 *Factor 1* is composed of a high proportion of particles in the nucleation range with a sharp mode at
669 ~15 nm. It accounts for 33% (32-35%) of PNC and less than 2% of PVC. The polar plot reveals
670 increased concentrations for moderate winds blowing from the airport sector and the diurnal pattern
671 is also compatible with the aircraft traffic. No statistically significant correlations are found with

any other monitored species (Table 3). Therefore, Factor 1 may be attributed to the airport emissions related to aircraft engine exhaust. As in the warm season, factor 1 is moderately correlated with factor 2 (fresh road traffic, $r=0.55$), indicating a quite clear relationship between the two sources.

Factor 2 represents particles in the 15-35 nm range of number concentration, accounting for 35% (33-37%) of total PNC (Figure 6; Table 1). Its importance for volume concentration is minimal (3%) with two modes at 30 and 200 nm. The diurnal pattern and the wind directionality are compatible with LHR as a source and it shows a weak positive correlation with NO_2 (0.42) and a strong correlation with nitrate (0.63) (Table 3). Despite its similarity and relationship with Factor 1 and the consequent similar potential origin, Factor 2 may represent a different source: Factors 1 and 2 remain clearly separated even at solutions down to 4 factors, demonstrating their structural robustness and the lack of potential artefacts affecting the PMF solution. Consequently, it can be concluded that they do not represent over-resolved solutions (i.e. factor splitting). The most plausible interpretation for Factor 2 is therefore the same as for the warm season, i.e. fresh road traffic emissions. Furthermore, this factor can be attributed to the road traffic generated by the airport and nearby major roads.

Factor 3 includes most of the particles in the Aitken range and accounts for 19% (18-20%) of PNC. Its contribution to particle volume concentration is relevant (9%) with a main peak at around 100 nm and a secondary peak at 400 nm (Table 1). It presents two rush hours peaks and the polar plot reveals an origin from the SW quadrant. However, as with the warm period, the wind directionality suggests increases for slower wind regimes than the fresh road traffic factor and for more westerly sectors, which are not compatible with the airfield location. Since factor 3 correlates well (Table 3) with a number of other pollutants linked to primary emissions from road traffic (NO (0.51), NO_2

697 (0.81), eBC (0.52), PM_{2.5} (0.53), OC (0.79) and EC (0.83)), it represents a second road traffic
 698 factor, more affected by aging in the atmosphere than factor 2.
 699
 700 Despite the wind regimes from NE sectors being poorly represented during the cold campaign,
 701 *Factor 4* is the only one showing a possible origin from London and for calm wind periods. As with
 702 the warm season, it is composed of a wide range of particles encompassing the Aitken and
 703 accumulation modes (50 to 150 nm), while the peak in volume concentration is at 170 nm (Table 1).
 704 The diurnal pattern (Figure 6) is clearly related to the mixing layer dynamics and the correlation
 705 analysis reveals strong relationships with many species (NO, NO₂, eBC, Delta-C, NVPM_{2.5}, OC,
 706 EC, nitrate, ammonium and potassium; Table 3). Consequently, it is concluded that it represents the
 707 urban accumulation mode, whose contribution to the total volume concentration is also similar to
 708 the warm season (33%). It is interesting to note the large similarity with the urban accumulation
 709 mode found in the warm season, from which it differs slightly only in the diurnal pattern (higher
 710 overnight) and in the presence of a strong correlation with nitrate ($r=0.88$), possibly due to the
 711 lesser extent of negative artefacts on PM_{2.5} filter samples.

712

713 The last two factors are interpreted as due to secondary aerosols. Their modal structures, their
 714 contributions to total PNC and PVC, and their correlations with PM_{2.5}-bound species (Table 3;
 715 Figure 6) largely reflect the results obtained for the warm period. However, the CWT maps (Figure
 716 7) highlight different source areas, i.e. the origin of the secondary aerosols is regional (UK and
 717 Northern Europe). In addition, the presence of strong positive correlations with chloride may also
 718 indicate a contribution from the transport of sea-salt aerosol.

719

720 **3.3 Comparison of *k*-means and PMF**

721 The cluster analysis revealed the presence of 5 characteristic PNSD shapes during both the seasons.
 722 These spectra have been linked to potential sources in the study area, i.e. road traffic, airport

723 activities, and secondary aerosol formation processes. However, the cluster analysis is mostly
724 driven by the spectral size regions with higher particle number concentrations, i.e. it has the
725 disadvantage of partitioning the single observations predominantly according to the finest region of
726 the size distribution. This limitation is well illustrated by the poor (almost null) separation of
727 clusters based on the particle volume distributions (all clusters showed quite similar particle volume
728 spectra). In addition, cluster analysis also has the disadvantage of linking each cluster to a single
729 source and does not easily account for PNSD resulting from the mix of two or more different
730 sources.

731

732 In contrast, the PMF analysis computed over the PNSD also accounts well for the sources with a
733 small impact on the number distribution, but having a larger influence on the particle volume size
734 distributions and, therefore, on the particle mass concentration. Despite the differences in the two
735 methods, some further information can be extracted by combining the results of cluster and PMF
736 analysis. Figure 8 shows the statistics of normalised PMF source contributions relating to each
737 single cluster.

738

739 For the warm period, significantly higher (0.05 significance) PMF contributions of the airport factor
740 (F1) are measured for cluster 1 (average normalised contribution ~ 3.5). This result indicates that the
741 airport fingerprint was well captured by both source apportionment methods. During the cold
742 season, the airport factor (F1) is significantly higher for both clusters 1 and 5 (average normalised
743 contributions of ~ 2 and ~ 3 , respectively). While cluster 5 presents significant high PMF
744 contributions only for factor 1, cluster 1 also shows high contributions of factor 2 (fresh road
745 traffic). This result indicates that cluster 5 may be linked as the typical PNSD spectra for airport
746 emissions, while cluster 2 likely represents mixed emissions from aircraft and airport-related traffic.
747 A close analysis of wind roses for the two clusters in the cold season (Figure 4) reveals that cluster
748 5 occurs at significantly higher wind speed regimes than cluster 1 (Mann-Whitney-Wilcoxon test at

0.05 significance level), i.e. average wind speeds of 8.3 and 5.9 m s⁻¹, respectively. As a consequence, the different wind regimes may well be responsible for the split between the two clusters.

Results for fresh traffic emissions also agree between the two methods. Factors 2 exhibit the higher normalised contributions to clusters 5 (normalised contribution 2.5) and 1 (normalised contribution ~3) for the warm and cold period, respectively (Figure 8). However, in winter it is evident that PNSDs grouped on cluster 1 are also strongly influenced by airport emissions, probably due to the lower mixing layer height and, thus, a lesser dispersion in the atmosphere.

Clusters 4 for both the periods show enrichments in the contributions for 4 PMF sources (aged road traffic, urban accumulation and the two secondary aerosols) (Figure 8). This further emphasises that cluster 4 represents the typical PNSD during daytime resulting from the mixing of different sources. In a similar way, clusters 3 and 2 in the warm and cold periods, respectively, represent the typical nighttime spectra (Figures 3 and 4), i.e. they exhibit similar partitioning over the PMF sources and similar daily cycles.

3.4 Analysis of a Large Regional Nucleation Event

Regional photochemical nucleation episodes are regularly recorded in the Southern and Eastern UK. Their general characteristics have been reported in a number of studies (e.g., Alam et al., 2003; Charron et al., 2007; 2008; Beddows et al., 2015; Vu et al., 2016) and can be summarised as follows: (i) particle modality at around 20 nm; (ii) higher frequency around noon in association with the peak in actinic flux intensities; (iii) clear seasonal cycles (higher average contribution levels in the summer, from June to September); (iv) marked directionality from the westerly sectors, reflecting maritime atmospheric circulation regimes, with high wind speed and low PM_{2.5} concentrations.

775 A strong regional nucleation event occurred during the warm period sampling campaign (starting on
 776 7th September at 1 pm UTC and lasting for about 12 h). Increases of PNC were almost
 777 simultaneously recorded at Harlington and at Harwell, a national network rural background site
 778 located approx. 60 km WNW of LHR and representative of the regional background levels of air
 779 pollution across the Southern UK. The comparison of PNC time series at the two sites is provided
 780 as Figure SI10. Figure 9 shows the contour plots of SMPS data recorded at Harlington between 7th
 781 and 8th September as well as the hourly averaged concentrations of nucleation, Aitken and
 782 accumulation particles, TEOM-FDMS PM_{2.5} mass and the contributions of Factors 1 to 4 extracted
 783 by the PMF. Figure 9 also reports the hourly counts of number of clusters extracted by the *k*-means
 784 analysis. The contour plot shows a typical “banana” shape with particle mode growing from ~20 nm
 785 (1 pm) to ~100 nm (overnight). The episode strongly influenced the PNSDs until around midnight;
 786 however its effect is also visible over the first half of 8th September. The time series (Figure 9)
 787 exhibits a clear peak in nucleation particles between 1 pm and 3 pm followed by peaks of Aitken (3-
 788 11 pm) and accumulation mode (8 pm-2 am) particles. The back-trajectory analysis (Figure SI11)
 789 revealed that the event occurred when north-westerly fresh (and clean) maritime air masses were
 790 advected from the Atlantic. This is also supported by the PM_{2.5} mass, which exhibited a fast drop of
 791 concentrations just a few hours before the event ($-30 \mu\text{g m}^{-3}$ in 3 hours, i.e. from $40 \mu\text{g m}^{-3}$ at 6 am
 792 to $10 \mu\text{g m}^{-3}$ at 9 am, Figure 9), probably reducing the condensation sink and facilitating nucleation.
 793
 794 Both atmospheric nucleation and aircraft engines are recognised to produce particles in the
 795 nucleation range. The analysis of this single –but strong– episode gives insights into how much the
 796 source apportionment results can potentially be affected by regional nucleation. This latter analysis
 797 is possible because the wind directionality during the entire episode was from N sectors, i.e. the
 798 contribution of LHR can be considered negligible.

799

800 The results of cluster analysis were affected by the event. Before the episode, the PNSD spectra
801 were mostly categorised as clusters 3 and 4 (urban background and daytime pollution, respectively),
802 i.e. the clusters mostly recorded under north-easterly wind regimes (Figure 3). About 50% and 30%
803 of the clusters were then categorised as “airport” in the first and second hour of the episode,
804 respectively (Figure 9). Since the wind directionality is inconsistent with an origin from the airfield,
805 this categorisation is likely the result of the nucleation event. The growing of particles in the hours
806 after the beginning of the event has further driven the cluster results: (i) about 60-80% of PNSDs
807 were categorised as “fresh road traffic” (cluster 5) after 2-3 hours, and (ii) 80-100% of PNSDs were
808 clustered as “nighttime regional pollution” (cluster 2) after 4-6 hours. In a similar way, PMF results
809 were affected by the event (Figure 9), with a sharp increase of contribution levels for: (i) factor 1
810 (airport) from 1.5×10^3 particles cm^{-3} at noon to 13.3×10^3 particles cm^{-3} at 2 pm; (ii) factor 2
811 (fresh road traffic) from 0.5×10^3 particles cm^{-3} at 1 pm to 21×10^3 particles cm^{-3} at 3 pm; and (iii)
812 factor 3 (aged road traffic) from 2.1×10^3 particles cm^{-3} at 2 pm to approx. 15×10^3 particles cm^{-3} at
813 5-6 pm.

814

815 This episode was the main nucleation event recorded during the two sampling campaigns. Other
816 possible episodes also occurred (mostly during the warm season), but they were much less
817 significant and often hard to detect. This qualitative analysis points to some conclusions: (i)
818 regional photochemical nucleation events may have an effect on clustering and PMF results; (ii) the
819 effect may lead to an “additive” bias, mostly over the “airport” and “road traffic” factors and
820 clusters; (iii) the effect of regional nucleation events in the study area is largely overwhelmed by the
821 strength of local sources, but in other locations with more frequent nucleation events it may be more
822 important to identify and separate them.

823

824

825

826 4 CONCLUSIONS

827 The effect of airport emissions upon the particle number concentration and size distribution was
828 assessed at a site close to a major European airport (Heathrow) serving a megacity (London). The
829 conclusions to be drawn are:

- 830 • High particle number concentrations were recorded for the finest sizes (nucleation <30 nm and
831 Aitken nuclei 30-100 nm) if compared to an urban background site in London (N. Kensington).
- 832 • Polar plot analysis indicates that Heathrow is a strong potential source for NO₂, nucleation and
833 Aitken particles, but its contribution to the mass concentration of PM_{2.5} and eBC is very small.
834 On the contrary, the urban area of London appears to be the main source for PM and eBC.
- 835 • The *k*-means cluster analysis has revealed that 20% of PNSDs are mostly shaped by airport
836 direct emissions, but particle size spectra are also strongly affected by other local sources
837 (mostly fresh and aged road traffic during daytime) and the reduction of mixing layer depth
838 (during nighttime). Typical PNSD spectra have been identified for nighttime and daytime
839 pollution as well. Such spectra are likely the result of multiple source mixtures.
- 840 • PMF analysis revealed that the fingerprint of Heathrow has a peculiar modal structure peaking
841 at <20 nm. The direct airport emissions account for 30-35% of total particles in both the
842 seasons. Such results are in line with percent estimations for NO₂ reported in previous studies.
- 843 • Other major contributors to PNC are fresh (24-36%) and aged (16-21%) road traffic emissions.
844 Despite both applied source apportionment methods failing to fully disaggregate the emissions
845 from the local traffic (including motorway) and traffic generated by the airport, results suggest
846 that road traffic sources may contribute to the total PNC more than Heathrow (40-56%).
847 However, making a clear distinction between the influence of traffic generated by the airport
848 from other road traffic is not feasible from this analysis.
- 849 • An urban accumulation mode was found. This source presents a wide mode between 50-150
850 nm and accounts for around 10% of PNC. The wind directionality is consistent with the
851 advection of air masses from London. It is more evident overnight due to the drop of the

852 mixing layer top, the subsequent increase in air pollutants at ground level and the generation of
853 nighttime secondary nitrate aerosols.

854 • Secondary sources accounted for less than 6% in number concentrations but for more than 50%
855 in volume concentration. Long-range transport has a key role in advecting polluted air masses
856 from mainland Europe.

858 **ACKNOWLEDGEMENTS**

859 This study was carried out under the Marie Skłodowska-Curie project ‘CHEERS’ (Chemical and
860 Physical Properties and Source Apportionment of Airport Emissions in the context of European Air
861 Quality Directives, call: FP7-PEOPLE-2012-IEF, project no. 328542). The authors gratefully
862 acknowledge: (i) the European Union for funding the Marie Curie Intra-European Fellowship for
863 career development to M. Masiol through the project ‘CHEERS’; (ii) Heathrow Airport Ltd and
864 Ricardo-AEA for supplying aircraft movement data and for the valuable exchange of information
865 and discussion, in particular Katherine Rolfe, Elizabeth Hegarty (Heathrow), Brian Stacey
866 (Ricardo-AEA) and David Vowles; (iii) DEFRA Automatic Urban and Rural Network, and London
867 Air Quality Network for providing pollutant data; (iv) Met Office and BADC for weather data; (v)
868 the NOAA Air Resources Laboratory (ARL) for the provision of the HYSPLIT transport and
869 dispersion model used in this publication; (vi) the UK Department for Transport, Road Traffic and
870 Road Freight Statistics, for providing M4 and M25 traffic data; and (vii) Dr. Stefania Squizzato
871 (University of Rochester, NY, USA) for the valuable exchange of information.

874 REFERENCES

- 875 ACI (Airport Council International): ACI releases preliminary world airport traffic rankings.
 876 Airports Council International, Montreal. Available at: [http://www.aci.aero/News/Releases/Most-](http://www.aci.aero/News/Releases/Most-Recent/2016/04/04/ACI-releases-preliminary-world-airport-traffic-rankings-)
 877 Recent/2016/04/04/ACI-releases-preliminary-world-airport-traffic-rankings- [last accessed: June
 878 2016].
 879
- 880 AEA: Heathrow Airport Air Quality Modelling for 2008/9: Results and Model Evaluation. Report
 881 by AEA Energy & Environment on behalf of BAA, July 2010. AEAT/ENV/R/2948/Issue 1.
 882
- 883 Al-Dabbous, A. N., Kumar, P.: Source apportionment of airborne nanoparticles in a Middle Eastern
 884 city using positive matrix factorization, *Environ. Sci. Process Impacts*, 17, 802-812, 2015.
 885
- 886 Alam, A., Shi, J. P. and Harrison, R. M.: Observations of new particle formation in urban air, *J.*
 887 *Geophys. Res.*, 108, 4093-4107, 2003. doi:10.1029/2001JD001417
 888
- 889 Anderson, B. E., Branham, H.-S., Hudgins, C. H., Plant, J. V., Ballenthin, J. O., Miller, T. M.,
 890 Viggiano, A. A., Blake, D. R., Boudries, H., Canagaratna, M., Miake-Lye, R. C., Onasch, T.,
 891 Wormhoudt, J., Worsnop, D., Brunke, K. E., Culler, S., Penko P., Sanders, T., Han, H.-S., Lee, P.,
 892 Pui, D. Y. H., Thornhill, K. L., Winstead, E. L.: Experiment to Characterize Aircraft Volatile
 893 Aerosol and Trace-Species Emissions (EXCAVATE), NASA/TM-2005-213783, National
 894 Aeronautics and Space Administration, Hampton, VA., 2005.
 895
- 896 Anttila, P., Tuovinen, J. P., Niemi, J. V.: Primary NO₂ emissions and their role in the development
 897 of NO₂ concentrations in a traffic environment, *Atmos. Environ.*, 45, 986-992, 2011.
 898
- 899 Atkinson, R. W., Fuller, G. W., Anderson, H. R., Harrison, R. M., Armstrong, B.: Urban ambient
 900 particle metrics and health: a time-series analysis, *Epidemiol.*, 21, 501-511, 2010.
 901
- 902 Beddows, D. C. S., Dall'Osto, M., Harrison, R. M.: Cluster analysis of rural, urban and curbside
 903 atmospheric particle size data, *Environ. Sci. Technol.*, 43, 4694-4700, 2009.
 904
- 905 Beddows, D. C. S., Dall'Osto, M., Harrison, R. M., Kulmala, M., Asmi, A., Wiedensohler, A., Laj,
 906 P., Fjaeraa, A. M., Sellegri, K., Birmili, W., Bukowiecki, N., Weingartner, E., Baltensperger, U.,
 907 Zdimal, V., Zikova, N., Putaud, J.-P., Marinoni, A., Tunved, P., Hansson, H.-C., Fiebig, M.,
 908 Kivekäs, N., Swietlicki, E., Lihavainen, H., Asmi, E., Ulevicius, V., Aalto, P. P., Mihalopoulos, N.,
 909 Kalivitis, N., Kalapov, I., Kiss, G., de Leeuw, G., Henzing, B., O'Dowd, C., Jennings, S. G., Flentje,
 910 H., Meinhardt, F., Ries, L., Denier van der Gon, H. A. C., Visschedijk, A. J. H.: Variations in
 911 tropospheric submicron particle size distributions across the European continent 2008-2009,
 912 *Atmos. Chem. Phys.*, 14, 4327-4348, 2014.
 913
- 914 Beddows D. C. S., Harrison R. M., Green D. C. and Fuller G. W.: Receptor modelling of both
 915 particle composition and size distribution from a background site in London, UK., *Atmos. Chem.*
 916 *Phys.*, 15, 10107-10125, 2015.
 917
- 918 Belis, C. A., Larsen, B. R., Amato, F., El Haddad, I., Favez, O., Harrison, R. M., Hopke, P. K.,
 919 Nava, S., Paatero, P., Prévôt, A., Quass, U., Vecchi, R. and Viana, M.: European guide on air
 920 pollution source apportionment with receptor models, JRC Reference Reports EUR26080 EN,
 921 2014.
 922

923 Benson, D. R., Yu, J. H., Markovich, A., Lee, S.-H.: Ternary homogeneous nucleation of H₂SO₄,
 924 NH₃, and H₂O under conditions relevant to the lower troposphere, *Atmos. Chem. Phys.*, 11, 4755-
 925 4766, 2011.

926 Bertram, T. H. and Thornton, J. A.: Toward a general parameterization of N₂O₅ reactivity on
 927 aqueous particles: the competing effects of particle liquid water, nitrate and chloride, *Atmos. Chem.*
 928 *Phys.*, 9, 8351-8363, 2009.

929

930 Bigi A and Harrison R. M.: Analysis of the air pollution climate at a central urban background site,
 931 *Atmos. Environ.*, 44, 2004-2012, 2010.

932

933 Brines, M., Dall'Osto, M., Beddows, D. C. S., Harrison, R. M. and Querol, X.: Simplifying aerosol
 934 size distributions modes simultaneously detected at four monitoring sites during SAPUSS, *Atmos.*
 935 *Chem. Phys.*, 14, 2973-2986, 2014.

936

937 Brines, M., Dall'Osto, M., Beddows, D., Harrison, R., Gómez-Moreno, F., Núñez, L., Artíñano, B.,
 938 Costabile, F., Gobbi, G. And Salimi, F.: Traffic and nucleation events as main sources of ultrafine
 939 particles in high-insolation developed world cities, *Atmos. Chem. Phys.*, 15, 5929-5945, 2015.

940

941 Brown, S. S. and Stutz, J.: Nighttime radical observations and chemistry, *Chem. Soc. Rev.*, 41,
 942 6405-6447, 2012.

943

944 Brown, S. G., Eberly, S., Paatero, P. and Norris, G. A.: Methods for estimating uncertainty in PMF
 945 solutions: Examples with ambient air and water quality data and guidance on reporting PMF results,
 946 *Sci.Total Environ.*, 518, 626-635, 2015.

947

948 Carslaw, D. C. and Ropkins, K.: Openair - an R package for air quality data analysis, *Environ.*
 949 *Model. Softw.*, 27-28, 52-61, 2012.

950

951 Carslaw, D. C., Beevers, S. D., Ropkins, K. and Bell, M. C.: Detecting and quantifying aircraft and
 952 other on-airport contributions to ambient nitrogen oxides in the vicinity of a large international
 953 airport, *Atmos. Environ.*, 40, 5424-5434, 2006.

954

955 Carslaw, D. C., Beevers, S. D. and Bell, M. C.: Risks of exceeding the hourly EU limit value for
 956 nitrogen dioxide resulting from increased road transport emissions of primary nitrogen dioxide,
 957 *Atmos. Environ.*, 41, 2073-2082, 2007.

958

959 Chandrasekaran, S. R., Hopke, P. K., Newtown, M. and Hurlbut, A.: Residential-scale biomass
 960 boiler emissions and efficiency characterization for several fuels, *Energy & Fuels*, 27, 4840-4849,
 961 2013.

962

963 Charron, A. and Harrison, R. M.: Primary particle formation from vehicle emissions during exhaust
 964 dilution in the roadside atmosphere, *Atmos. Environ.*, 37, 4109-4119, 2003.

965

966 Charron, A., Degrendele, C., Laongsri, B. and Harrison, R. M.: Receptor modelling of secondary
 967 and carbonaceous particulate matter at a southern UK site, *Atmos. Chem. Phys.* 13, 1879-1894,
 968 2013.

969

970 Charron, A., Birmili, W. and Harrison, R. M.: Factors influencing new particle formation at the rural
 971 site, Harwell, United Kingdom, *J. Geophys. Res.*, 112, D14210, 2007. doi:10.1029/2007JD008425.

972

973

974 Charron, A., Birmili, W. and Harrison, R. M.: Fingerprinting particle origins according to their size
975 distribution at a UK rural site, *J. Geophys. Res.*, 113, D07202, 2008. doi:10.1029/2007JD008562.
976

977 Chen, J. P., Tsai, T. S. and Liu, S. C.: Aerosol nucleation spikes in the planetary boundary layer,
978 *Atmos. Chem. Phys.*, 11, 7171-7184, 2011.
979

980 Cheung, H. C., Morawska, L., Ristovski, Z. D., and Wainwright, D.: Influence of medium range
981 transport of particles from nucleation burst on particle number concentration within the urban
982 airshed, *Atmos. Chem. Phys.*, 12, 4951-4962, 2012.
983

984 Clapp, L. J. and Jenkin, M. E.: Analysis of the relationship between ambient levels of O₃, NO₂ and
985 NO as a function of NO_x in the UK, *Atmos. Environ.*, 35, 6391-6405, 2001.
986

987 Costabile, F., Birmili, W., Klose, S., Tuch, T., Wehner, B., Wiedensohler, A., Franck, U.,
988 König, K. and Sonntag, A.: Spatio-temporal variability and principal components of the particle
989 number size distribution in an urban atmosphere, *Atmos. Chem. Phys.*, 9, 3163-3195, 2009.
990

991 Cyrys, J., Eeftens, M., Heinrich, J., Ampe, C., Armengaud, A., Beelen, R., Bellander, T.,
992 Beregszaszi, T., Birk, M., Cesaroni, G., Cirach, M., de Hoogh, K., De Nazelle, A., de Vocht, F.,
993 Declercq C., Dedele, A., Dimakopoulou, K., Eriksen, K., Galassi, C., Grauleviciene, R., Grivas, G.,
994 Gruzjeva, O., Hagenbjörk Gustafsson, A., Hoffmann, B., Iakovides, M., Ineichen, A., Krämer, U.,
995 Lanki, T., Lozano, P., Madsen, C., Meliefste, K., Modig, L., Mölterm, A., Mosler, G.,
996 Nieuwenhuijsen, M., Nonnemacher, M., Oldenwening, M., Peters, A., Pontet, S., Probst-Hensch,
997 N., Quass, U., Raaschou-Nielsen, O., Ranzi, A., Sugiri, D., Stephanou, E.G., Taimisto, P., Tsai, M.-
998 Y., Vaskövi, E., Villani, S., Wang, M., Brunekreef, B. and Hoek, G.: Variation of NO₂ and NO_x
999 concentrations between and within 36 European study areas: Results from the ESCAPE study,
1000 *Atmos. Environ.*, 62, 374-390, 2012.
1001

1002 Dall'Osto, M., Harrison, R. M., Coe, H., Williams, P. I. and Allan, J.D.: Real time chemical
1003 characterization of local and regional nitrate aerosols, *Atmos. Chem. Phys.*, 9, 3709-3720, 2009.
1004

1005 Dall'Osto, M., Thorpe, A., Beddows, D. C. S., Harrison, R. M., Barlow, J. F., Dunbar, T., Williams,
1006 P.I. and Coe, H.: Remarkable dynamics of nanoparticles in the urban atmosphere, *Atmos. Chem.*
1007 *Phys.*, 11, 6623-6637, 2011.
1008

1009 Dall'Osto, M., Beddows, D. C. S., Pey, J., Rodriguez, S., Alastuey, A., Harrison, R. M. and Querol,
1010 X.: Urban aerosol size distributions over the Mediterranean city of Barcelona, NE Spain, *Atmos.*
1011 *Chem. Phys.*, 12, 10693-10707, 2012.
1012

1013 DEFRA: Air Pollution in the UK 2015. UK Department for Environment, Food and Rural Affairs.
1014 Issue of September 2016. Available at: [https://uk-](https://uk-air.defra.gov.uk/assets/documents/annualreport/air_pollution_uk_2015_issue_1.pdf)
1015 [air.defra.gov.uk/assets/documents/annualreport/air_pollution_uk_2015_issue_1.pdf](https://uk-air.defra.gov.uk/assets/documents/annualreport/air_pollution_uk_2015_issue_1.pdf) (last accessed:
1016 November 2016).
1017

1018 Dodson, R. E., Houseman, E. A., Morin, B. and Levy, J. I.: An analysis of continuous black carbon
1019 concentrations in proximity to an airport and major roadways, *Atmos. Environ.*, 43, 3764-3773,
1020 2009.
1021

1022 Farias, F. and ApSimon, H.: Relative contributions from traffic and aircraft NO_x emissions to
1023 exposure in West London, *Environ. Modell. Softw.*, 21, 477-485, 2006.
1024

1025 Finlayson-Pitts, B. J. and Pitts Jr, J. N.: Chemistry of the upper and lower atmosphere: theory,
 1026 experiments, and applications. Academic press, 2000.
 1027

1028 Grice, S., Stedman, J., Kent, A., Hobson, M., Norris, J., Abbott, J., Cooke S.: Recent trends and
 1029 projections of primary NO₂ emissions in Europe, *Atmos. Environ.*, 43, 2154-2167, 2009.
 1030

1031 Harrison, R. M., Beddows, D. C. S. and Dall'Osto, M.: PMF Analysis of wide-range particle size
 1032 spectra collected on a major highway, *Environ. Sci. Technol.*, 45, 5522-5528, 2011.
 1033

1034 Harrison, R.M., Dall'Osto, M., Beddows, D.C.S., Thorpe, A.J., Bloss, W.J., Allan, J.D., Coe, H.,
 1035 Dorsey, J.R., Gallagher, M., Martin, C. and Whitehead, J.: Atmospheric chemistry and physics in
 1036 the atmosphere of a developed megacity (London): an overview of the REPARTEE experiment and
 1037 its conclusions. *Atmos. Chem. Phys.*, 12(6), 3065-3114, 2012.
 1038

1039 Harrison, R. M., Beddows, D. C., Jones, A. M., Calvo, A., Alves, C. and Pio, C.: An evaluation of
 1040 some issues regarding the use of aethalometers to measure woodsmoke concentrations, *Atmos.*
 1041 *Environ.*, 80, 540-548, 2013.
 1042

1043 Harrison, R. M., Jones, A. M., Beddows, D. C. S., Dall'Osto, M. and Nikolova, I.: Evaporation of
 1044 traffic-generated nanoparticles during advection from source, *Atmos. Environ.*, 125, 1-7, 2016.
 1045

1046 Herndon, S. C., Jayne, J. T., Lobo, P., Onasch, T. B., Fleming, G., Hagen, D. E., Whitefield, P. D.
 1047 and Miake-Lye, R. C.: Commercial aircraft engine emissions characterization of in-use aircraft at
 1048 Hartsfield-Jackson Atlanta International Airport, *Environ. Sci. Technol.*, 42, 1877-1883, 2008.
 1049

1050 Hopke, P. K.: Review of receptor modeling methods for source apportionment. *JAWMA*, 66, 237-
 1051 259, 2016.
 1052

1053 Hsu, H.H., Adamkiewicz, G., Houseman, E.A., Vallarino, J., Melly, S.J., Wayson, R.L., Spengler,
 1054 J.D. and Levy, J.I.: The relationship between aviation activities and ultrafine particulate matter
 1055 concentrations near a mid-sized airport, *Atmos. Environ.*, 50, 328-337, 2012a.
 1056

1057 Hsu, H.H., Adamkiewicz, G., Houseman, E.A., Vallarino, J., Melly, S.J., Wayson, R.L., Spengler,
 1058 J.D. and Levy, J.I.: The relationship between aviation activities and ultrafine particulate matter
 1059 concentrations near a mid-sized airport, *Atmos. Environ.*, 50, 328-337, 2012b.
 1060

1061 Hsu, H. H., Adamkiewicz, G., Houseman, E. A., Zarubiak, D., Spengler, J. D. and Levy, J. I.:
 1062 Contributions of aircraft arrivals and departures to ultrafine particle counts near Los Angeles
 1063 International Airport, *Sci. Tot. Environ.*, 444, 347-355, 2013.
 1064

1065 Hsu, H. H., Adamkiewicz, G., Houseman, E. A., Spengler, J. D., Levy and J.I.: Using mobile
 1066 monitoring to characterize roadway and aircraft contributions to ultrafine particle concentrations
 1067 near a mid-sized airport, *Atmos. Environ.*, 89, 688-695, 2014.
 1068

1069 Hu, S., Fruin, S., Kozawa, K., Mara, S., Winer, A.M. and Paulson, S.E.: Aircraft emission impacts
 1070 in a neighborhood adjacent to a general aviation airport in Southern California, *Environ. Sci.*
 1071 *Technol.*, 43(21), 8039-8045, 2009.
 1072

1073 Hudda, N., Gould, T., Hartin, K., Larson, T. V. and Fruin, S. A.: Emissions from an international
 1074 airport increase particle number concentrations 4-fold at 10 km downwind, *Environ. Sci. Technol.*,
 1075 48, 6628-6635, 2014.
 1076

1077 Hudda, N., Simon, M. C., Zamore, W., Brugge, D. And Durant, J. L.: Aviation emissions impact
 1078 ambient ultrafine particle concentrations in the greater Boston area, *Environ.Sci. Technol.*, 50,
 1079 8514-8521, 2016.
 1080
 1081 Hudda, N., Fruin, S.A.: International airport impacts to air quality: size and related properties of
 1082 large increases in ultrafine particle number concentrations, *Environ. Sci. Technol.*, 50, 3362-3370,
 1083 2016.
 1084
 1085 Hussein, T., Molgaard, B., Hannuniemi, H., Martikainen, J., Jarvi, L., Wegner, T., Ripamonti, G.,
 1086 Weber, S., Vesala, T. and Hameri, K.: Fingerprints of the urban particle number size distribution in
 1087 Helsinki, Finland: local vs. regional characteristics, *Boreal Env. Res.*, 19, 1-20, 2014.
 1088
 1089 ICAO (International Civil Aviation Organization), Annual Report of the ICAO Council: 2014. The
 1090 World of Air Transport in 2014, Appendix 1: [https://www.icao.int/annual-report-](https://www.icao.int/annual-report-2014/Documents/Appendix_1_en.pdf)
 1091 [2014/Documents/Appendix_1_en.pdf](https://www.icao.int/annual-report-2014/Documents/Appendix_1_en.pdf), last access: 20 June 2017.
 1092
 1093 Janhäll S., Jonsson Å. M., Molnár P., Svensson E. A. and Hallquist M.: Size resolved traffic
 1094 emission factors of submicrometer particles, *Atmos. Environ.*, 38, 4331-4340, 2004.
 1095
 1096 Jones, A.M., Harrison, R.M., Barratt, B. and Fuller, G.: A large reduction in airborne particle
 1097 number concentrations at the time of the introduction of “sulphur free” diesel and the London Low
 1098 Emission Zone, *Atmos. Environ.*, 50, 129-138, 2012.
 1099
 1100 Kasumba, J., Hopke, P. K., Chalupa, D. C. and Utell, M. J.: Comparison of sources of submicron
 1101 particle number concentrations measured at two sites in Rochester, NY, *Sci. Total Environ.*, 407,
 1102 5071-5084, 2009.
 1103
 1104 Kelly, F. J. and Fussell, J. C.: Size, source and chemical composition as determinants of toxicity
 1105 attributable to ambient particulate matter, *Atmos. Environ.*, 60, 504-526, 2012.
 1106 Kerminen, V. M., Pirjola, L., Boy, M., Eskola, A., Teinilä, K., Laakso, L., Asmi, A., Hienola, J.,
 1107 Lauri, A., Vainio, V. And Lehtinen, K.: Interaction between SO₂ and submicron atmospheric
 1108 particles, *Atmos. Res.*, 54, 41-57, 2000.
 1109
 1110 Keuken, M. P., Moerman, M., Zandveld, P., Henzing, J. S. and Hoek, G.: Total and size-resolved
 1111 particle number and black carbon concentrations in urban areas near Schiphol airport (the
 1112 Netherlands), *Atmos. Environ.*, 104 132-142, 2015.
 1113
 1114 Kim, E., Hopke, P. K., Larson, T. V. and Covert, D. S.: Analysis of ambient particle size
 1115 distributions using unmix and positive matrix factorization, *Environ. Sci. Technol.*, 38, 202-209,
 1116 2004.
 1117
 1118 Kinsey, J. S., Dong, Y., Williams, D. C. and Logan, R.: Physical characterization of the fine
 1119 particle emissions from commercial aircraft engines during the aircraft particle emissions
 1120 experiment (APEX) 1 to 3, *Atmos. Environ.*, 44, 2147-2156, 2010.
 1121
 1122 Klapmeyer, M.E. and Marr, L.C.: CO₂, NO_x, and Particle Emissions from Aircraft and Support
 1123 Activities at a Regional Airport, *Environ. Sci. Technol.*, 46(20), 10974-10981, 2012.
 1124
 1125 Kley, D., Kleinmann, M., Sanderman, H. and Krupa, S.: Photochemical oxidants: state of the
 1126 science, *Environ. Pollut.*, 100, 19-42, 1999.
 1127

Knibbs, L. D., Cole-Hunter, T. and Morawska, L.: A review of commuter exposure to ultrafine particles and its health effects, *Atmos. Environ.*, 45, 2611-2622, 2011.

Kruskal, W.H. and Wallis, W.A., Use of ranks in one-criterion variance analysis. *J. Amer. Statist. Assoc.*, 47, 583-621, 1952.

Kulmala, M., Toivonen, A., Mäkelä, J. M. and Laaksonen, A.: Analysis of the growth of nucleation mode particles observed in Boreal forest, *Tellus B*, 50, 449-462, 1998.

Kulmala, M. and Kerminen, V.-M.: On the formation and growth of atmospheric nanoparticles, *Atmos. Res.*, 90, 132–150, 2008.

Kumar, P., Morawska, L., Birmili, W., Paasonen, P., Hu, M., Kulmala, M., Harrison, R. M., Norford, L. and Britter, R.: Ultrafine particles in cities, *Environ.Int.*, 66, 1-10, 2014.

Kumar, P., Pirjola, L., Ketzel, M. and Harrison, R M.: Nanoparticle emissions from 11 non-vehicle exhaust sources—A review, *Atmos.Environ.*, 67, 252-277, 2013.

Lanzinger, S., Schneider, A., Breitner, S., Stafoggia, M., Erzen, I., Dostal, M., Pastorkova, A., Bastian, S., Cyrus, J., Zscheppang, A. and Kolodnitska, T.: Associations between ultrafine and fine particles and mortality in five central European cities—Results from the UFIRES study, *Environ. Int.*, 88, 44-52, 2016.

Lee, D. S., Fahey, D. W., Forster, P. M., Newton, P. J., Wit, R. C. N., Lim, L. L., Owen, B., Sausen and R.: Aviation and global climate change in the 21st century, *Atmos. Environ.*, 43, 3520-3537, 2009.

Liu, X., Wang, W., Liu, H., Geng, C., Zhang, W., Wang, H. and Liu, Z.: Number size distribution of particles emitted from two kinds of typical boilers in a coal-fired power plant in China, *Eng. Fuels*, 24, 1677-1681, 2010.

Liu, Z. R., Hu, B., Liu, Q., Sun, Y. and Wang, Y. S.: Source apportionment of urban fine particle number concentration during summertime in Beijing, *Atmos. Environ.*, 96, 359-369, 2014.

Lobo, P., Hagen, D. E. and Whitefield, P. D.: Measurement and analysis of aircraft engine PM emissions downwind of an active runway at the Oakland International Airport, *Atmos. Environ.*, 61, 114-123, 2012.

Lobo, P., Hagen, D. E., Whitefield, P. D. and Raper, D.: PM emissions measurements of in-service commercial aircraft engines during the Delta-Atlanta Hartsfield Study, *Atmos. Environ.*, 104, 237-245, 2015.

Lupu, A. and Maenhaut, W.: Application and comparison of two statistical trajectory techniques for identification of source regions of atmospheric aerosol species, *Atmos. Environ.*, 36, 5607-5618, 2002.

Masiol, M. and Harrison, R. M.: Aircraft engine exhaust emissions and other airport-related contributions to ambient air pollution: A review, *Atmos. Environ.*, 95, 409-455, 2014.

Masiol, M. and Harrison, R.M.: Quantification of air quality impacts of London Heathrow Airport (UK) from 2005 to 2012, *Atmos. Environ.*, 116, 308-319, 2015.

1180 Masiol, M., Vu, V. T., Beddows, D. C. S. and Harrison, R.M.: Source apportionment of wide range
 1181 particle size spectra and black carbon collected at the airport of Venice (Italy), *Atmos. Environ.*,
 1182 139, 56-74, 2016.

1183

1184 Masiol M., Hopke P. K., Felton H. D., Frank B. P., Rattigan O. V., Wurth M. J. and LaDuke G. H.:
 1185 Source apportionment of PM_{2.5} chemically speciated mass and particle number concentrations in
 1186 New York City, *Atmos. Environ.*, 148, 215-229, 2017.

1187

1188 Mazaheri, M., Johnson, G. R. and Morawska, L.: Particle and gaseous emissions from commercial
 1189 aircraft at each stage of the landing and takeoff cycle, *Environ. Sci. Technol.*, 43, 441-446, 2009.

1190

1191 Mazaheri, M., Bostrom, T. E., Johnson, G. R. and Morawska, L.: Composition and morphology of
 1192 particle emissions from in-use aircraft during takeoff and landing, *Environ. Sci. Technol.*, 47, 5235-
 1193 5242, 2013.

1194

1195 Meyer, N. K. and Ristovski, Z.: Ternary nucleation as a mechanism for the production of diesel
 1196 nanoparticles: experimental analysis of the volatile and hygroscopic properties of diesel exhaust
 1197 using the volatilization and humidification tandem differential mobility analyser, *Environ. Sci.*
 1198 *Technol.*, 41, 7309-7314, 2007.

1199

1200 Ntziachristos, L., Ning, Z. Geller, M. D. and Sioutas, C.: Particle concentration and characteristics
 1201 near a major freeway with heavy-duty diesel traffic, *Environ. Sci. Technol.*, 41, 2223-2230, 2007.

1202

1203 O'Dowd, C. D., Geever, M., Hill, M. K., Smith, M. H. and Jennings, S. G.: New particle formation:
 1204 Nucleation rates and spatial scales in the clean marine coastal environment, *Geophys. Res. Lett.*, 25,
 1205 1661-1664, 1998.

1206

1207 O'Dowd, C., McFiggans, G., Creasey, D. J., Pirjola, L., Hoell, C., Smith, M. H., Allan, B. J., Plane,
 1208 J. M. C., Heard, D. E., Lee, J. D., Pilling, M. J. and Kulmala, M.: On the photochemical production
 1209 of new particles in the coastal boundary layer. *Geophys. Res. Lett.*, 26, 1707-1710, 1999.

1210

1211 Ogulei, D., Hopke, P. K., Chalupa, D. C. and Utell, M. J.: Modeling source contributions to
 1212 submicron particle number concentrations measured in Rochester, New York, *Aerosol Sci.*
 1213 *Technol.*, 41, 179-201, 2007.

1214 Ostro, B., Hu, J., Goldberg, D., Reynolds, P., Hertz, A., Bernstein, L. and Kleeman, M. J.:
 1215 Associations of mortality with long-term exposures to fine and ultrafine particles, species and
 1216 sources: Results from the California Teachers Study Cohort, *Environ. Health Perspect.*, 123, 549-
 1217 556, 2015.

1218

1219 Paatero, P.: Least squares formulation of robust non-negative factor analysis, *Chemom. Intell. Lab.*,
 1220 37, 23-35, 1997.

1221

1222 Paatero, P. and Tapper, U.: Positive matrix factorization: a non-negative factor model with optimal
 1223 utilization of error estimates of data values, *Environmetrics*, 5, 111-126, 1994.

1224

1225 Paatero, P., Hopke, P. K., Song, X. H. and Ramadan, Z.: Understanding and controlling rotations in
 1226 factor analytic models, *Chemom. Intell. Lab. Syst.*, 60, 253-264, 2002.

1227

1228 Paatero, P., Eberly, S., Brown, S. G. and Norris, G. A.: Methods for estimating uncertainty in
 1229 factor analytic solutions., *Atmos. Meas. Tech.*, 7, 781-797, 2014.

1230

1231 Pant, P. and Harrison, R. M.: Estimation of the contribution of road traffic emissions to particulate
 1232 matter concentrations from field measurements: a review, *Atmos. Environ.*, 77, 78-97, 2013.
 1233
 1234 Petzold, A., Ogren, J.A., Fiebig, M., Laj, P., Li, S.M., Baltensperger, U., Holzer-Popp, T., Kinne,
 1235 S., Pappalardo, G., Sugimoto, N. and Wehrli, C., Wiedensohler, A., Zhang, X.-Y.:
 1236 Recommendations for reporting "black carbon" measurements, *Atmos. Chem. Phys.*, 13, 8365-
 1237 8379, 2013.
 1238
 1239 R Core Team: R: A language and environment for statistical computing. R Foundation for
 1240 Statistical Computing, Vienna, Austria, 2015. URL <http://www.R-project.org/>.
 1241
 1242 Reff, A., Eberly, S. I. and Bhawe, P. V.: Receptor modeling of ambient particulate matter data using
 1243 positive matrix factorization: review of existing methods, *JAWMA*, 57, 146-154, 2007.
 1244
 1245 Ren, J., Liu, J., Li, F., Cao, X., Ren, S., Xu, B. and Zhu, Y.: A study of ambient fine particles at
 1246 Tianjin International Airport, China, *Sci. Total Environ.*, 556, 126-135, 2016.
 1247
 1248 Riccobono, F., Schobesberger, S., Scott, C. E., Dommen, J., Ortega, I. K., Rondo, L., Almeida, J.,
 1249 Amorim, A., Bianchi, F., Breitenlechner, M. And David, A.: Oxidation products of biogenic
 1250 emissions contribute to nucleation of atmospheric particles, *Science*, 344, 717-721, 2014.
 1251
 1252 Rolph, G. D.: Real-time Environmental Applications and Display sYstem (READY) Website,
 1253 <http://www.ready.noaa.gov>, NOAA Air Resources Laboratory, College Park, MD, 2016.
 1254
 1255 Salimi, F., Ristovski, Z., Mazaheri, M., Laiman, R., Crilley, L. R., He, C., Clifford, S. and
 1256 Morawska, L.: Assessment and application of clustering techniques to atmospheric particle number
 1257 size distribution for the purpose of source apportionment, *Atmos. Chem. Phys.*, 14, 11883-11892,
 1258 2014.
 1259
 1260 Salma, I., Fűri, P., Németh, Z., Balásházy, I., Hofmann, W. and Farkas, Á.: Lung burden and
 1261 deposition distribution of inhaled atmospheric urban ultrafine particles as the first step in their
 1262 health risk assessment, *Atmos. Environ.*, 104, 39-49, 2015.
 1263
 1264 Sandradewi, J., Prévôt, A. S., Szidat, S., Perron, N., Alfarra, M. R., Lanz, V. A., Weingartner, E.
 1265 and Baltensperger, U.: Using aerosol light absorption measurements for the quantitative
 1266 determination of wood burning and traffic emission contributions to particulate matter, *Environ.*
 1267 *Sci. Technol.*, 42, 3316-3323, 2008.
 1268
 1269 Schneider, J., Hock, N., Weimer, S., Borrmann, S., Kirchner, U., Vogt, R. and Scheer, V.:
 1270 Nucleation particles in diesel exhaust: Composition inferred from in situ mass spectrometric
 1271 analysis, *Environ. Sci. Technol.*, 39, 6153-6161, 2005.
 1272
 1273 Seinfeld, J. H. and Pandis, S. N.: *Atmospheric Chemistry and Physics - From Air Pollution to*
 1274 *Climate Change*, second ed., John Wiley & Sons, New York, 2006.
 1275
 1276 Shi, J. P. and Harrison, R. M.: Investigation of ultrafine particle formation during diesel exhaust
 1277 dilution, *Environ. Sci. Technol.*, 33, 3730-3736, 1999.
 1278
 1279 Shi, L., Zanobetti, A., Kloog, I., Coull, B. A., Koutrakis, P., Melly, S. J. and Schwartz, J. D.: Low-
 1280 concentration PM_{2.5} and mortality: Estimating acute and chronic effects in a population-based
 1281 study, *Environ. Health Perspect.*, 124, 46-52, 2015.
 1282

1283 Shirmohammadi, F., Sowlat, M. H., Hasheminassab, S., Saffari, A., Ban-Weiss, G. and Sioutas, C.:
 1284 Emission rates of particle number, mass and black carbon by the Los Angeles International Airport
 1285 (LAX) and its impact on air quality in Los Angeles, *Atmos. Environ.*, 151, 82-93, 2017.
 1286
 1287 Sowlat M.H., Hasheminassab S. and Sioutas C.: Source apportionment of ambient particle number
 1288 concentrations in central Los Angeles using positive matrix factorization (PMF), *Atmos. Chem.*
 1289 *Phys.*, 16, 4849-4866, 2016.
 1290
 1291 Squizzato, S. and Masiol, M.: Application of meteorology-based methods to determine local and
 1292 external contributions to particulate matter pollution: A case study in Venice (Italy), *Atmos.*
 1293 *Environ.*, 119, 69-81, 2015.
 1294
 1295 Stein, A. F., Draxler, R. R., Rolph, G. D., Stunder, B. J. B., Cohen, M. D. and Ngan, F.: NOAA's
 1296 HYSPLIT atmospheric transport and dispersion modeling system, *Bull. Amer. Meteor. Soc.*, 96,
 1297 2059-2077, 2015.
 1298
 1299 Stevens, R. G., Pierce, J. R., Brock, C. A., Reed, M. K., Crawford, J. H., Holloway, J. S., Ryerson,
 1300 T. B., Huey, L. G. and Nowak, J. B.: Nucleation and growth of sulfate aerosol in coal-fired power
 1301 plant plumes: sensitivity to background aerosol and meteorology, *Atmos. Chem. Phys.*, 12, 189-
 1302 206, 2012.
 1303
 1304 Stohl A.: Trajectory statistics—a new method to establish source–receptor relationships of air
 1305 pollutants and its application to the transport of particulate sulfate in Europe, *Atmos. Environ.*, 30,
 1306 579-587, 1996.
 1307
 1308 Stohl, A.: Computation, accuracy and applications of trajectories- review and bibliography, *Atmos.*
 1309 *Environ.*, 32, 947-966, 1998.
 1310
 1311 Stafoggia, M., Cattani, G., Forastiere, F., di Bucchianico, A. D. M., Gaeta, A. And Ancona, C.:
 1312 Particle number concentrations near the Rome-Ciampino city airport, *Atmos. Environ.*, 147, 264-
 1313 273, 2016.
 1314
 1315 Strak, M. M., Janssen, N. A., Godri, K. J., Gosens, I., Mudway, I. S., Cassee, F. R., Lebret, E.,
 1316 Kelly, F. J., Harrison, R. M., Brunekreef, B. and Steenhof, M.: Respiratory health effects of
 1317 airborne particulate matter: the role of particle size, composition, and oxidative potential-the
 1318 RAPTES project, *Environ. Health Perspect.*, 120, 1183-1189, 2012.
 1319
 1320 Thimmaiah, D., Hovorka, J. and Hopke, P. K.: Source apportionment of winter submicron Prague
 1321 aerosols from combined particle number size distribution and gaseous composition data. *Aerosol*
 1322 *Air Qual.Res.*, 9, 209-236, 2009.
 1323
 1324 Turner, J.R., Hansen, A.D.A., and Allen G.A.: Methodologies to compensate for optical saturation
 1325 and scattering in aethalometer black carbon measurements, in: *Proceedings from the Symposium on*
 1326 *Air Quality Measurement Methods and Technology*, San Francisco, CA, USA, 30 April-3 May
 1327 2007, Air and Waste Management Association, 2007.
 1328
 1329 UK Department for Transport, Heathrow Airport expansion:
 1330 <https://www.gov.uk/government/collections/heathrow-airport-expansion>, last access: 20 June
 1331 2017.
 1332
 1333 USEPA: EPA Positive Matrix Factorization (PMF) 5.0 - Fundamentals and user guide.
 1334 EPA/600/R-14/108, 2014

1335
1336 Virkkula, A., Mäkelä, T., Hillamo, R., Yli-Tuomi, T., Hirsikko, A., Hämeri, K. and Koponen, I.K.:
1337 A simple procedure for correcting loading effects of aethalometer data, *J. Air Waste Manage.*
1338 *Assoc.*, 57, 1214-1222, 2007.

1339
1340 Vogt, R., Scheer, V., Casati, R. and Benter, T.: Onroad measurement of particle emission in the
1341 exhaust plume of a diesel passenger car, *Environ. Sci. Technol.*, 37, 4070-4076, 2003.

1342
1343 von Bismarck-Osten, C., Birmili, W., Ketzel, M., Massling, A., Petäjä, T. and Weber, S.:
1344 Characterization of parameters influencing the spatio-temporal variability of urban particle number
1345 size distributions in four European cities, *Atmos. Environ.*, 77, 415-429, 2013.

1346
1347 Vu, T. V., Delgado-Saborit, J. M. and Harrison, R. M.: A review of hygroscopic growth factors of
1348 submicron aerosols from different sources and its implication for calculation of lung deposition
1349 efficiency of ambient aerosols, *Air Quality, Atmos. Health*, 8, 429-440, 2015a.

1350
1351 Vu, T. V., Delgado-Saborit, J. M. and Harrison, R. M.: Review: Particle number size distributions
1352 from seven major sources and implications for source apportionment studies, *Atmos. Environ.*, 122,
1353 114-132, 2015b.

1354
1355 Vu, T. V., Beddows, D. C. S., Delgado-Saborit, J. M. and Harrison, R. M.: Source Apportionment
1356 of the Lung Dose of Ambient Submicrometre Particulate Matter, *Aerosol Air Quality Res.*, doi:
1357 10.4209/aaqr.2015.09.0553, 2016

1358
1359 Yin, J., Harrison, R. M., Chen, Q., Rutter, A. and Schauer, J. J.: Source apportionment of fine
1360 particles at urban background and rural sites in the UK atmosphere, *Atmos. Environ.*, 44, 841-851,
1361 2010.

1362
1363 Yue, W., Stolzel, M., Cyrys, J., Pitz, M., Heinrich, J., Kreyling, W. G., Wichmann, H.-E., Peters, A.,
1364 Wang, S. and Hopke, P.K.: Source apportionment of ambient fine particle size distribution using
1365 positive matrix factorization in Erfurt, Germany, *Sci. Total Environ.*, 398, 133-144, 2008.

1366
1367 Wang, Y., Hopke, P. K., Rattigan, O. V., Xia, X., Chalupa, D. C., Utell, M. J.: Characterization of
1368 residential wood combustion particles using the two-wavelength aethalometer, *Environ.Sci.*
1369 *Technol.*, 45, 7387-7393, 2011.

1370
1371 Webb, S., Whitefield, P. D., Miake-Lye, R. C., Timko, M. T. and Thrasher, T. G.: Research needs
1372 associated with particulate emissions at airports, ACRP Report 6, Transportation Research Board,
1373 Washington, D.C., 2008.

1374
1375 Wehner, B., Uhrner, U., Von Löwis, S., Zallinger, M. and Wiedensohler, A.: Aerosol number size
1376 distributions within the exhaust plume of a diesel and a gasoline passenger car under on-road
1377 conditions and determination of emission factors, *Atmos. Environ.*, 43, 1235-1245, 2009.

1378
1379 Wegner, T., Hussein, T., Hämeri, K., Vesala, T., Kulmala, M. and Weber, S.: Properties of aerosol
1380 signature size distributions in the urban environment as derived by cluster analysis, *Atmos.*
1381 *Environ.*, 61, 350-360, 2012.

1382
1383 Westerdahl, D., Fruin, S.A., Fine, P.L. and Sioutas, C.: The Los Angeles International Airport as a
1384 source of ultrafine particles and other pollutants to nearby communities, *Atmos. Environ.*, 42(13),
1385 3143-3155, 2008.

1386

1387 Wormhoudt, J., Herndon, S. C., Yelvington, P. E., Lye-Miake, R. C. and Wey, C.: Nitrogen oxide
 1388 (NO/NO₂/HONO) emissions measurements in aircraft exhausts, *J. Propul. Power*, 23, 906-911,
 1389 2007.
 1390
 1391 Zhang, K. M., Wexler, A. S., Zhu, Y. F., Hinds, W. C. and Sioutas, C.: Evolution of particle
 1392 number distribution near roadways. Part II: the 'Road-to-Ambient' process, *Atmos. Environ.*, 38,
 1393 6655-6665, 2004.
 1394
 1395 Zhang, K. M., Wexler, A. S., Niemeier, D. A., Zhu, Y. F., Hinds, W. C. and Sioutas, C.: Evolution
 1396 of particle number distribution near roadways. Part III: Traffic analysis and on-road size resolved
 1397 particulate emission factors, *Atmos. Environ.*, 39, 4155-4166, 2005.
 1398
 1399 Zhang, R., Khalizov, A., Wang, L., Hu, M. and Xu, W.: Nucleation and growth of nanoparticles in
 1400 the atmosphere, *Chem. Rev.*, 112, 1957-2011, 2011.
 1401
 1402 Zhou, L., Hopke, P. K., Stanier, C. O., Pandis, S. N., Ondov, J. M. and Pancras, J. P.: Investigation
 1403 of the relationship between chemical composition and size distribution of airborne particles by
 1404 partial least squares and positive matrix factorization, *J. Geophys. Res.-Atmos.*, 110, D07S18, 2005,
 1405 doi:10.1029/2004JD005050.
 1406
 1407 Zíková, N., Wang, Y., Yang, F., Li, X., Tian, M. and Hopke, P. K.: On the source contribution to
 1408 Beijing PM 2.5 concentrations, *Atmos. Environ.*, 134, 84-95, 2016.
 1409
 1410

1411 **TABLE LEGENDS:**

1412

1413 **Table 1.** Summary of PMF results for both seasons.

1414

1415 **Table 2.** Results of Pearson's correlation analysis among extracted factor contributions and
 1416 other measured variables recorded at different time resolutions. Only correlations
 1417 significant at $p < 0.05$ are reported, strong correlations ($\rho > |0.6|$) are highlighted in bold.

1418

1419

1420 **FIGURE LEGENDS:**

1421

1422 **Figure 1.** Statistics of size distribution spectra for particle number (red) and volume (blue)
 1423 concentrations categorised by sampling periods and time of the day (daytime= 7am-
 1424 7pm and nighttime=7pm- 7am local time). For the particle number spectra, solid lines
 1425 represent the median concentrations, while shaded areas report the 1st-3rd quartile
 1426 intervals (interquartile range, IQR). For the particle volume spectra, only medians are
 1427 reported (dotted lines).

1428

1429 **Figure 2.** Diurnal patterns of PNC, LHR traffic, solar irradiance and eBC. Plots report the
 1430 average levels as a filled line and the associated 95th confidence interval calculated by
 1431 bootstrapping the data ($n = 200$). Outliers (data > 99.5 th percentile) were removed for
 1432 computing the diurnal patterns. Hours are given in UTC. LHR traffic movements
 1433 (bottom right plot) are reported as arrivals (dotted lines) and departures (solid lines).
 1434 The offset between the seasons is largely due to daylight saving time (BST = UTC +
 1435 1) in the summer data. The diurnal patterns of all the measured variables in reported in
 1436 Figure SI4.

1437

1438 **Figure 3.** Results of cluster analysis for the warm season data. Average cluster PNSD spectra
 1439 (left) are reported as solid red lines along with: (i) their 10th, 25th, 75th and 90th
 1440 percentile spectrum as shaded areas; (ii) the volume size distributions (dotted blue
 1441 line); (iii) the hourly counts and (iv) the wind roses associated with each cluster.

1442

1443 **Figure 4.** Results of cluster analysis for the cold season data. Average cluster PNSD spectra
 1444 (left) are reported as solid red lines along with: (i) their 10th, 25th, 75th and 90th
 1445 percentile spectrum as shaded areas; (ii) the volume size distributions (dotted blue
 1446 line); (iii) the hourly counts and (iv) the wind roses associated with each cluster.

1447

1448 **Figure 5.** Results of PMF analysis for the warm season data. Factor profiles are reported on the
 1449 left as: (i) number concentration in solid red lines; (ii) their DISP ranges in shaded red
 1450 areas; (iii) volume concentrations in dotted blue lines; (iv) explained variation in
 1451 dashed grey lines. The plots on the centre report the normalised daily patterns
 1452 calculated on the hourly-averaged factor contributions along with their 95th
 1453 confidence intervals ($n = 200$ bootstrap). The plots on the right show the polar plot
 1454 analysis (normalised average factor contributions). SA=secondary aerosol.

1455

1456 **Figure 6.** Results of PMF analysis for the cold season data. Factor profiles are reported on the
 1457 left as: (i) number concentration in solid red lines; (ii) their DISP ranges in shaded red
 1458 areas; (iii) volume concentrations in dotted blue lines; (iv) explained variation in
 1459 dashed grey lines. The plots on the centre report the normalised daily patterns
 1460 calculated on the hourly-averaged factor contributions along with their 95th

confidence intervals (n=200 bootstrap). The plots on the right show the polar plot analysis (normalised average factor contributions). SA=secondary aerosol.

Figure 7. CWT maps of the secondary aerosol-related factors for both the seasons. Map scales refer to the average factor contributions to the total variable (PNC).

Figure 8. Comparison of k-means and PMF for the warm (upper plots) and cold (bottom plots) seasons. Boxplot statistics: lines= medians, crosses= arithmetic means, boxes= 25th-75th percentile ranges, whiskers= ± 1.5 *inter-quartile ranges.

Figure 9. Analysis of the regional nucleation episode occurring on September 7th. The selected period is from 7 September midnight to 8 September 4 pm. The plots represent (from upper to the bottom): (a) contour plots of SMPS data; (b) Concentrations of some measured species (Nucl= particles in the nucleation range 14-30 nm; Ait= particles in the Aitken Nuclei range 30-100 nm; Acc= particles in the accumulation range >100 nm; mass of PM_{2.5}); (c) Source contributions from PMF for the Factors 1, 2, 3 and 4; (d) hourly counts of number of clusters. The arrows in the (b) and (c) plots show the wind direction (arrow direction) and speed (proportional to arrow length).

1481 **Table 1.** Summary of PMF results for both seasons.

1482

| Factor number and interpretation | Particle Number Concentration | | Particle Volume Concentration | |
|--|--|-----------------------------------|--|----------------------|
| | No. modes ^a (peak ranges ^b) | Percent contribution (DISP range) | No. modes ^a (peak ranges ^b) | Percent contribution |
| Warm season (Aug-Sep 2014) | | | | |
| Factor 1: Airport | 1 (<20 nm) | 31.6 (30.8–36.2) | 2 (60–160 nm; <25 nm) | 1.2 |
| Factor 2: Fresh road traffic | 1 (20–35 nm) | 27.9 (24.7–30.2) | 2 (22–45 nm; 140–220 nm) | 1.7 |
| Factor 3: Aged road traffic | 1 (30–60 nm) | 18.9 (16.6–21.1) | 2 (40–100 nm; 250–450 nm) | 5.6 |
| Factor 4: Urban accumulation | 1 (50–150 nm) | 14.4 (13.8–18) | 1 (80–250 nm) | 33.2 |
| Factor 5: Mixed SA^c | 1 (110–250 nm) | 5.2 (3.6–6.9) | 1 (160–350 nm) | 37.4 |
| Factor 6: Inorganic SA | 2 (55–120 nm; 230–400 nm) | 2.1 (1.1–3.5) | 2 (260–500 nm; 75–140 nm) | 20.8 |
| Cold season (Dec 2014-Jan 2015) | | | | |
| Factor 1: Airport | 1 (<20 nm) | 33.1 (31.7–34.8) | 2 (160–350 nm; 15–25 nm) | 1.7 |
| Factor 2: Fresh road traffic | 1 (18–35 nm) | 35.2 (33.4–36.9) | 2 (22–45 nm; 150–300 nm) | 3.1 |
| Factor 3: Aged road traffic | 1 (28–60 nm) | 18.9 (17.9–19.7) | 2 (40–150 nm; 330–450 nm) | 8.7 |
| Factor 4: Urban accumulation | 1 (55–170 nm) | 7.6 (7.3–8.3) | 1 (100–250 nm) | 32.5 |
| Factor 5: Mixed SA | 2 (130–280 nm, <17 nm) | 2.3 (2.1–3.3) | 1 (170–400 nm) | 30.8 |
| Factor 6: Inorganic SA | 3 (17–28 nm; 55–100 nm, 250–400 nm) | 2.9 (2.4–3.9) | 2 (280–550 nm; 90–140 nm) | 23.3 |

(a) Only modes above the DISP ranges are shown; (b) Range endpoints are taken at approx. half the mode height;

(c) SA = secondary aerosol

1483

Table 2. Results of Pearson's correlation analysis among extracted factor contributions and other measured variables recorded at different time resolutions. Only correlations significant at $p < 0.05$ are reported, strong correlations ($\rho > |0.6|$) are highlighted in bold.

| Variables | Warm period | | | | | |
|---|-------------|--------------------|-------------------|--------------------|-------------|--------------|
| | Factor 1 | Factor 2 | Factor 3 | Factor 4 | Factor 5 | Factor 6 |
| | Airport | Fresh road traffic | Aged road traffic | Urban accumulation | Mixed SA | Inorganic SA |
| <i>Weather parameters (1 h-resolution time)</i> | | | | | | |
| Solar irr. | 0.12 | -0.15 | -0.24 | -0.26 | -0.24 | -0.28 |
| Air temp. | 0.25 | -0.21 | -0.37 | -0.1 | 0.1 | |
| RH | | 0.1 | 0.32 | 0.22 | 0.26 | 0.33 |
| Wind speed | 0.38 | | -0.47 | -0.64 | -0.45 | -0.49 |
| <i>5 min-resolution time</i> | | | | | | |
| Factor 1 | – | | | | | |
| Factor 2 | 0.46 | – | | | | |
| Factor 3 | 0.03 | 0.28 | – | | | |
| Factor 4 | -0.17 | -0.04 | 0.47 | – | | |
| Factor 5 | -0.15 | -0.06 | 0.21 | 0.56 | – | |
| Factor 6 | -0.17 | -0.14 | 0.15 | 0.56 | 0.75 | – |
| eBC | -0.1 | -0.03 | 0.33 | 0.62 | 0.52 | 0.53 |
| Delta-C | | | 0.13 | -0.07 | | -0.06 |
| <i>1 h-resolution time</i> | | | | | | |
| NO | | | 0.43 | 0.6 | 0.32 | 0.33 |
| NO ₂ | | 0.18 | 0.61 | 0.76 | 0.52 | 0.52 |
| NO _x | | 0.11 | 0.58 | 0.77 | 0.48 | 0.48 |
| O ₃ | 0.14 | -0.19 | -0.57 | -0.54 | -0.37 | -0.43 |
| PM _{2.5} | -0.23 | -0.24 | 0.13 | 0.61 | 0.63 | 0.77 |
| NVPM _{2.5} | -0.22 | -0.22 | 0.17 | 0.62 | 0.61 | 0.75 |
| VPM _{2.5} | -0.17 | -0.24 | | 0.42 | 0.54 | 0.65 |
| <i>1 day-resolution time PM_{2.5}-bound species</i> | | | | | | |
| OC | | | | 0.84 | 0.74 | 0.83 |
| EC | -0.47 | -0.54 | | 0.75 | 0.51 | 0.67 |
| TC | -0.45 | -0.44 | | 0.85 | 0.69 | 0.82 |
| Chloride | | | | | | |
| Nitrate | | -0.45 | | | 0.83 | 0.85 |
| Sulphate | | -0.57 | | 0.75 | 0.5 | 0.67 |
| Oxalate | | -0.47 | | 0.59 | 0.89 | 0.93 |
| Sodium | | | | | | |
| Ammonium | -0.44 | -0.52 | | 0.57 | 0.54 | 0.71 |
| Potassium | | -0.47 | | 0.46 | 0.5 | 0.66 |
| Magnesium | 0.5 | | | -0.53 | | |
| Calcium | | | | | | |

1489 **Table 2.** Continued.

1490

| Variables | Factor 1 | Factor 2 | Cold period | | Factor 5 | Factor 6 |
|---|----------|--------------------|-------------------|--------------------|--------------|--------------|
| | Airport | Fresh road traffic | Aged road traffic | Urban accumulation | Mixed SA | Inorganic SA |
| <i>Weather parameters (1 h-resolution time)</i> | | | | | | |
| Solar irr. | | | | -0.11 | | |
| Air temp. | 0.38 | | -0.43 | -0.67 | -0.5 | -0.59 |
| RH | | | 0.23 | 0.38 | 0.46 | 0.46 |
| Wind speed | 0.3 | | -0.49 | -0.67 | -0.54 | -0.61 |
| <i>5 min-resolution time</i> | | | | | | |
| Factor 1 | – | | | | | |
| Factor 2 | 0.55 | – | | | | |
| Factor 3 | 0.24 | 0.54 | – | | | |
| Factor 4 | -0.11 | 0.08 | 0.53 | – | | |
| Factor 5 | -0.05 | 0.15 | 0.38 | 0.65 | – | |
| Factor 6 | -0.09 | 0.08 | 0.39 | 0.7 | 0.81 | – |
| eBC | | 0.16 | 0.52 | 0.77 | 0.60 | 0.63 |
| Delta-C | | | 0.35 | 0.62 | 0.55 | 0.52 |
| <i>1 h-resolution time</i> | | | | | | |
| NO | -0.14 | | 0.51 | 0.81 | 0.62 | 0.63 |
| NO ₂ | 0.13 | 0.42 | 0.81 | 0.82 | 0.61 | 0.66 |
| NO _x | | 0.17 | 0.63 | 0.85 | 0.64 | 0.68 |
| O ₃ | | -0.29 | -0.71 | -0.78 | -0.65 | -0.7 |
| PM _{2.5} | -0.1 | 0.16 | 0.53 | 0.82 | 0.88 | 0.88 |
| NVPM _{2.5} | -0.11 | 0.16 | 0.53 | 0.82 | 0.85 | 0.85 |
| VPM _{2.5} | | | 0.19 | 0.39 | 0.49 | 0.48 |
| <i>1 day-resolution time PM_{2.5}-bound species</i> | | | | | | |
| OC | | | 0.79 | 0.79 | 0.76 | 0.8 |
| EC | | | 0.83 | 0.8 | 0.64 | 0.66 |
| TC | | | 0.81 | 0.8 | 0.73 | 0.77 |
| Chloride | | | | 0.58 | 0.82 | 0.85 |
| Nitrate | | 0.63 | 0.73 | 0.88 | 0.93 | 0.9 |
| Sulphate | | | | | 0.92 | 0.88 |
| Oxalate | | | | | 0.87 | 0.81 |
| Sodium | | -0.58 | -0.74 | -0.64 | | |
| Ammonium | | | 0.63 | 0.78 | 0.99 | 0.97 |
| Potassium | | | | 0.71 | 0.98 | 0.97 |
| Magnesium | | | | | | |
| Calcium | | | | | | |

1491

1492

1493

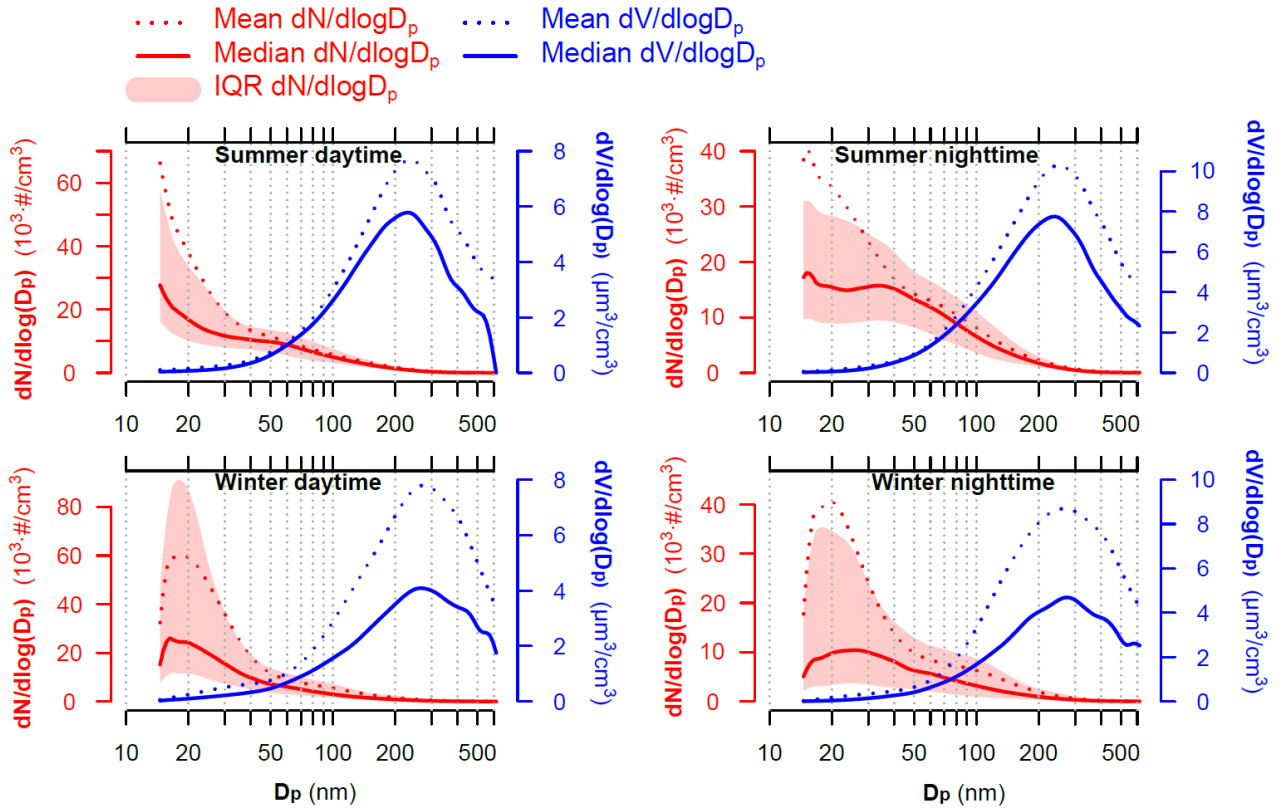


Figure 1. Statistics of size distribution spectra for particle number (red) and volume (blue) concentrations categorised by sampling periods and time of the day (daytime= 7am-7pm and nighttime=7pm- 7am local time). For the particle number spectra, solid lines represent the median concentrations, while shaded areas report the 1st-3rd quartile intervals (interquartile range, IQR). For the particle volume spectra, only medians are reported (dotted lines).

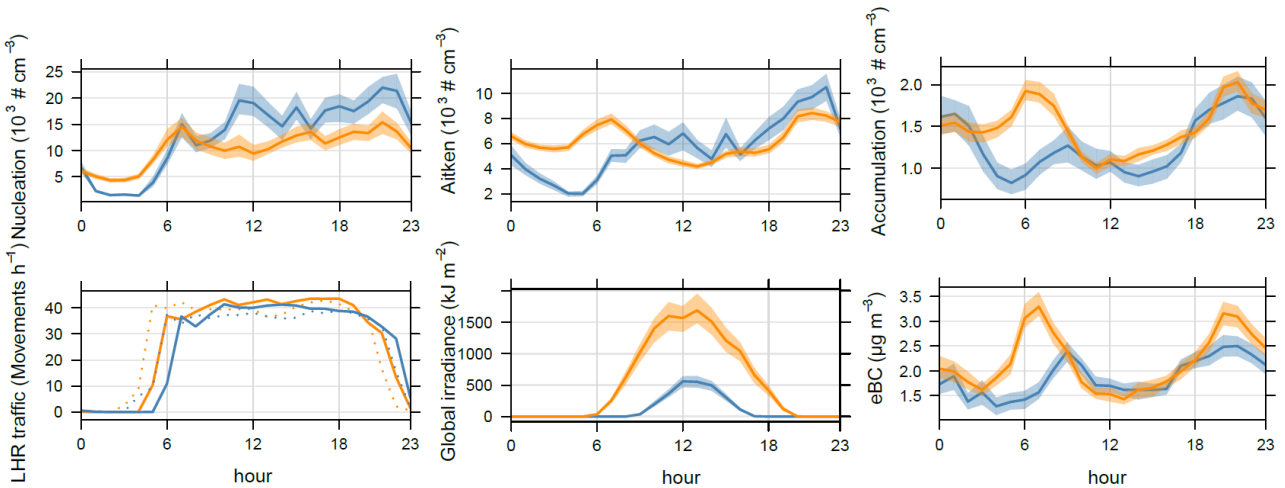
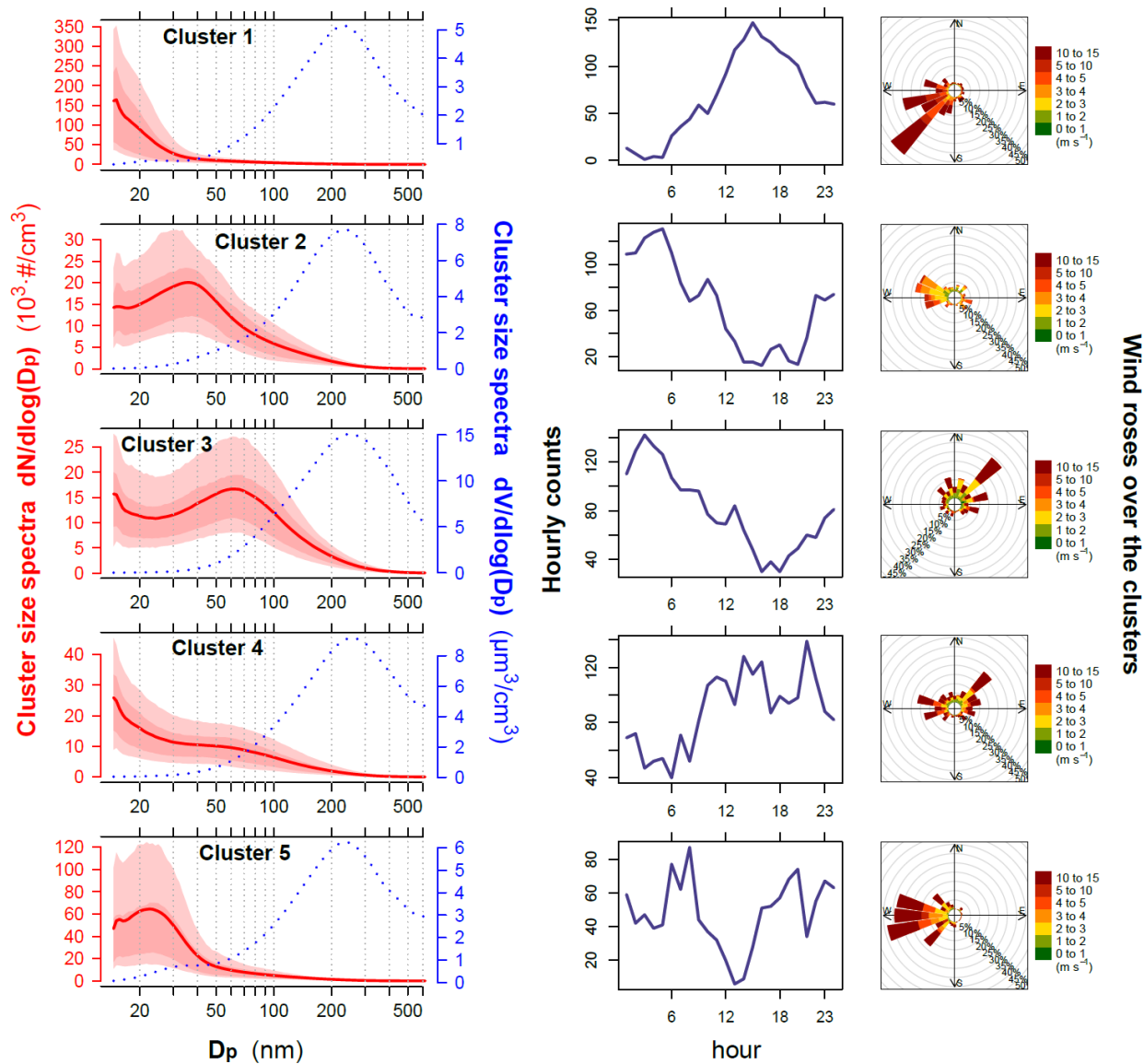


Figure 2. Diurnal patterns of PNC, LHR traffic, solar irradiance and eBC. Plots report the average levels as a filled line and the associated 95th confidence interval calculated by bootstrapping the data ($n=200$). Outliers (data >99.5 th percentile) were removed for computing the diurnal patterns. Hours are given in UTC. LHR traffic movements (bottom right plot) are reported as arrivals (dotted lines) and departures (solid lines). The offset between the seasons is largely due to daylight saving time (BST = UTC + 1) in the summer data. The diurnal patterns of all the measured variables in reported in Figure SI4.



1511

1512

1513

1514

1515

Figure 3. Results of cluster analysis for the warm season data. Average cluster PNSD spectra (left) are reported as solid red lines along with: (i) their 10th, 25th, 75th and 90th percentile spectrum as shaded areas; (ii) the volume size distributions (dotted blue line); (iii) the hourly counts and (iv) the wind roses associated with each cluster.

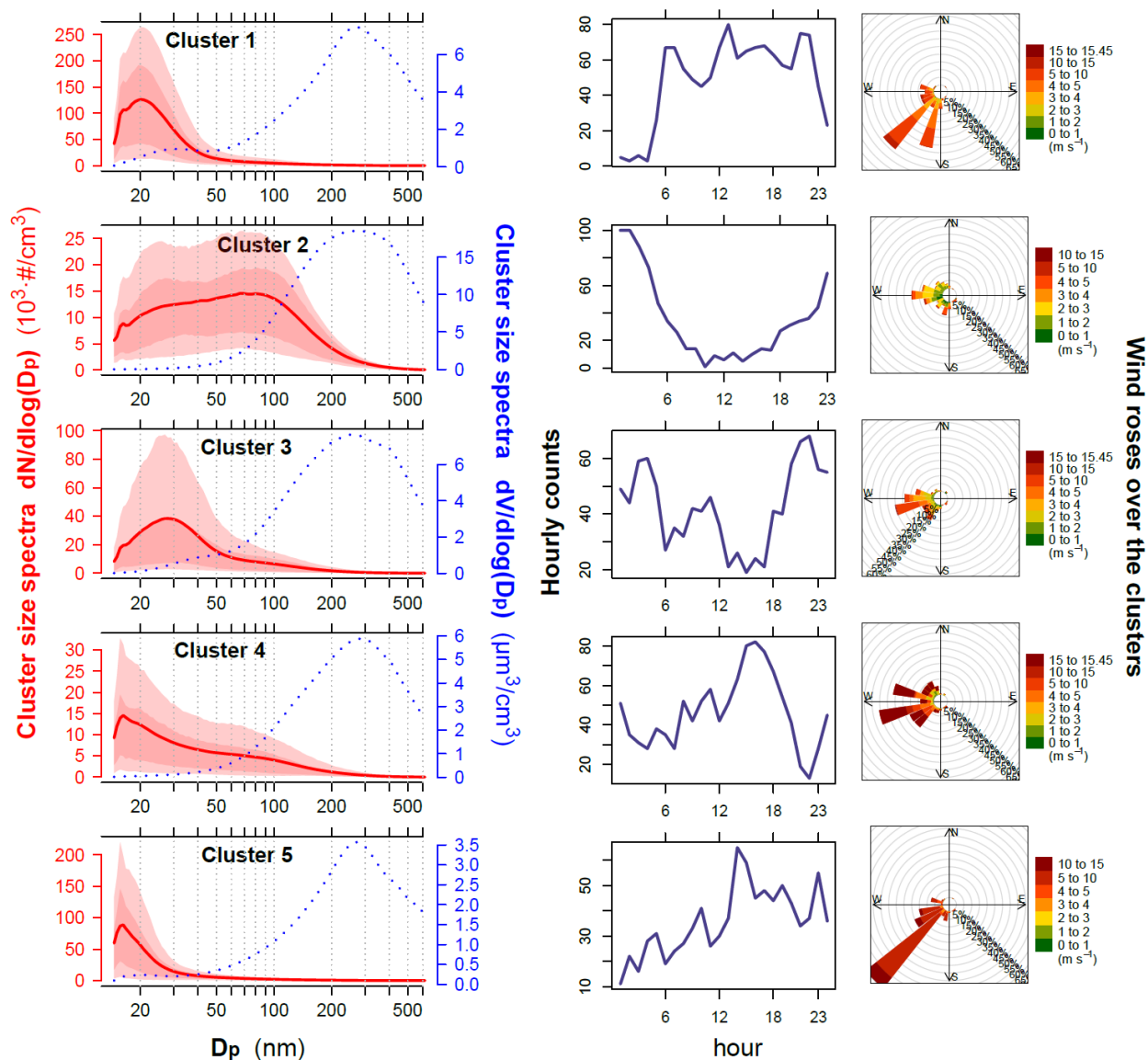


Figure 4. Results of cluster analysis for the cold season data. Average cluster PNSD spectra (left) are reported as solid red lines along with: (i) their 10th, 25th, 75th and 90th percentile spectrum as shaded areas; (ii) the volume size distributions (dotted blue line); (iii) the hourly counts and (iv) the wind roses associated with each cluster.

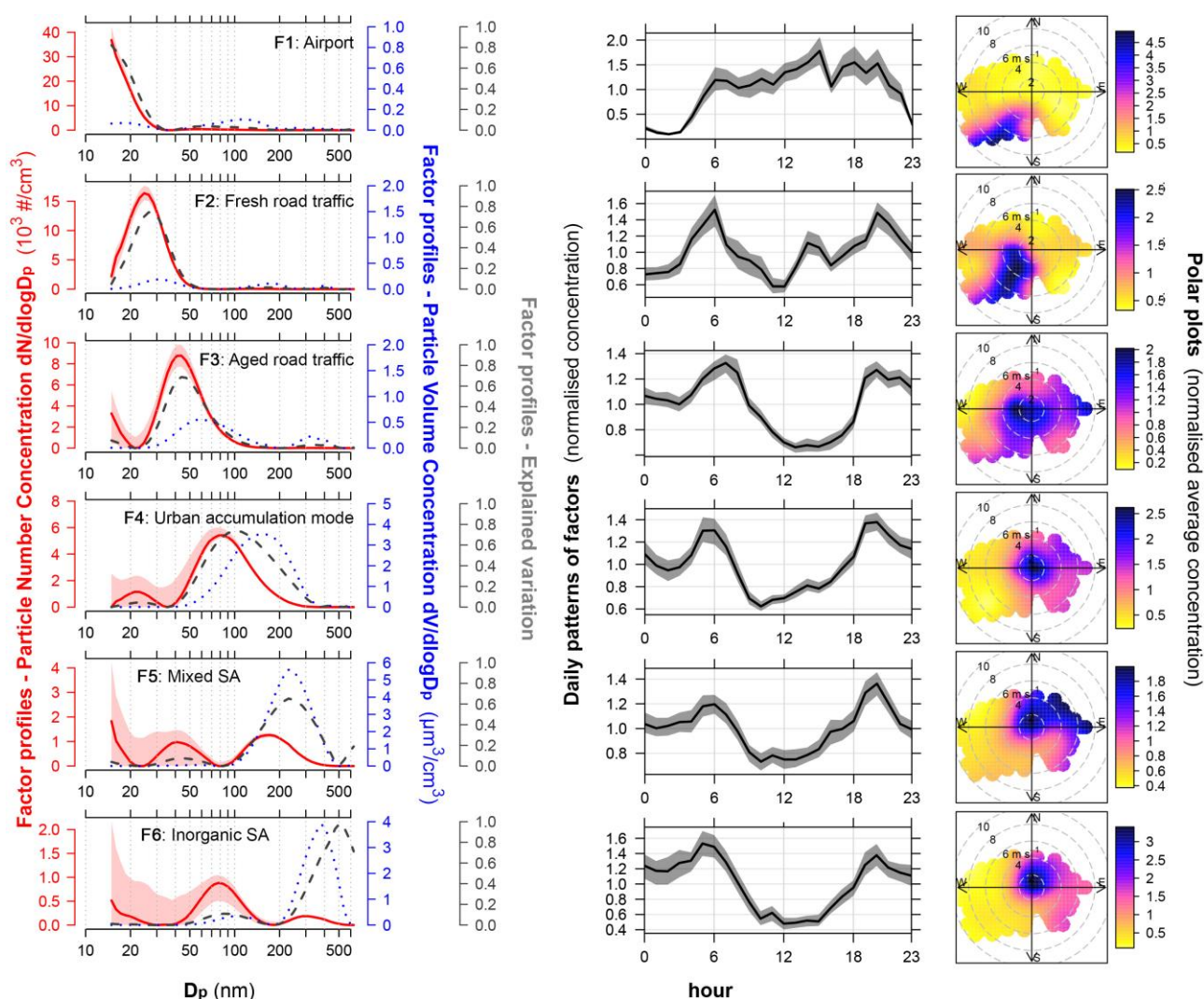


Figure 5. Results of PMF analysis for the warm season data. Factor profiles are reported on the left as: (i) number concentration in solid red lines; (ii) their DISP ranges in shaded red areas; (iii) volume concentrations in dotted blue lines; (iv) explained variation in dashed grey lines. The plots on the centre report the normalised daily patterns calculated on the hourly-averaged factor contributions along with their 95th confidence intervals ($n=200$ bootstrap). The plots on the right show the polar plot analysis (normalised average factor contributions). SA=secondary aerosol.

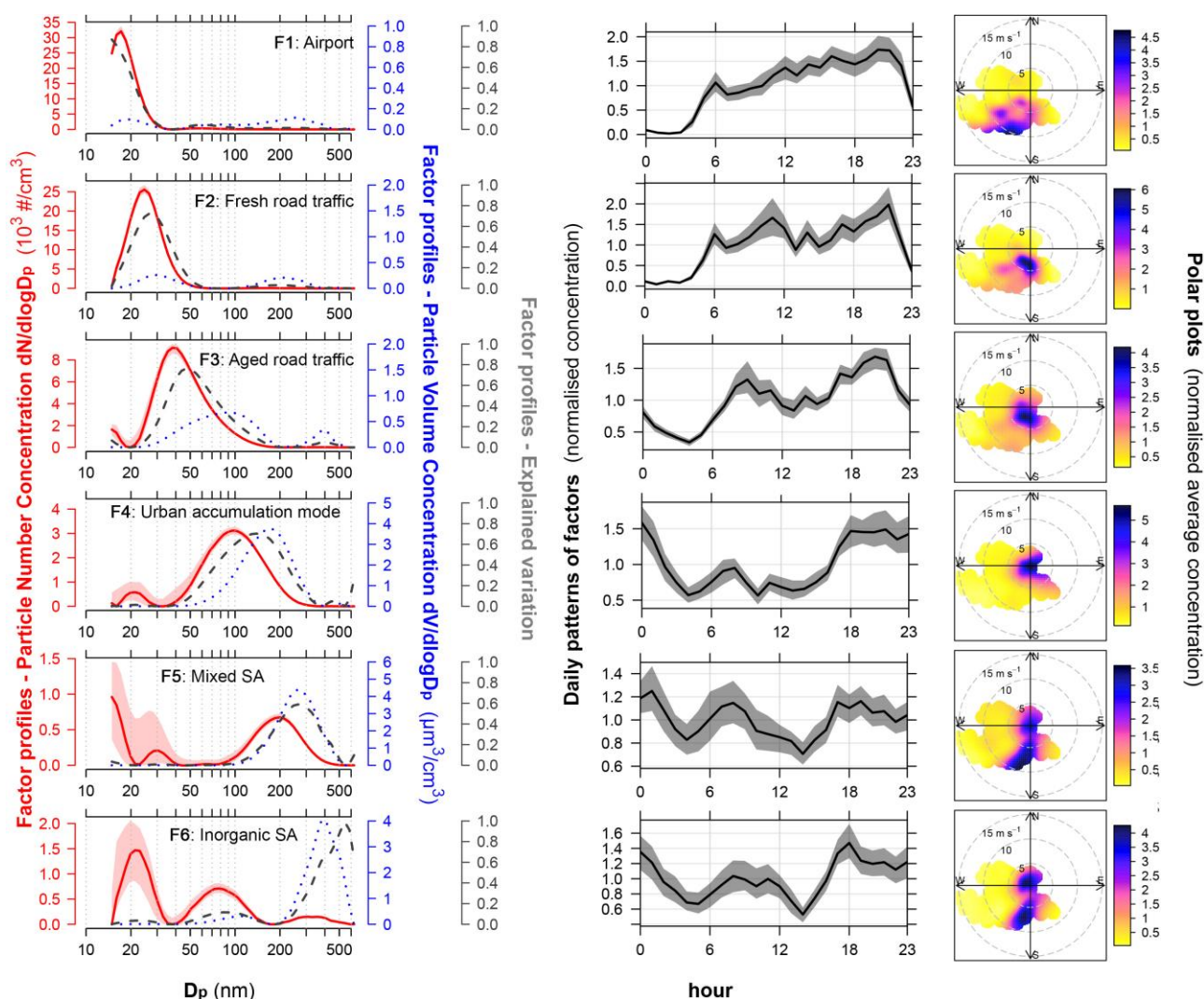


Figure 6. Results of PMF analysis for the cold season data. Factor profiles are reported on the left as: (i) number concentration in solid red lines; (ii) their DISP ranges in shaded red areas; (iii) volume concentrations in dotted blue lines; (iv) explained variation in dashed grey lines. The plots on the centre report the normalised daily patterns calculated on the hourly-averaged factor contributions along with their 95th confidence intervals ($n=200$ bootstrap). The plots on the right show the polar plot analysis (normalised average factor contributions). SA=secondary aerosol.

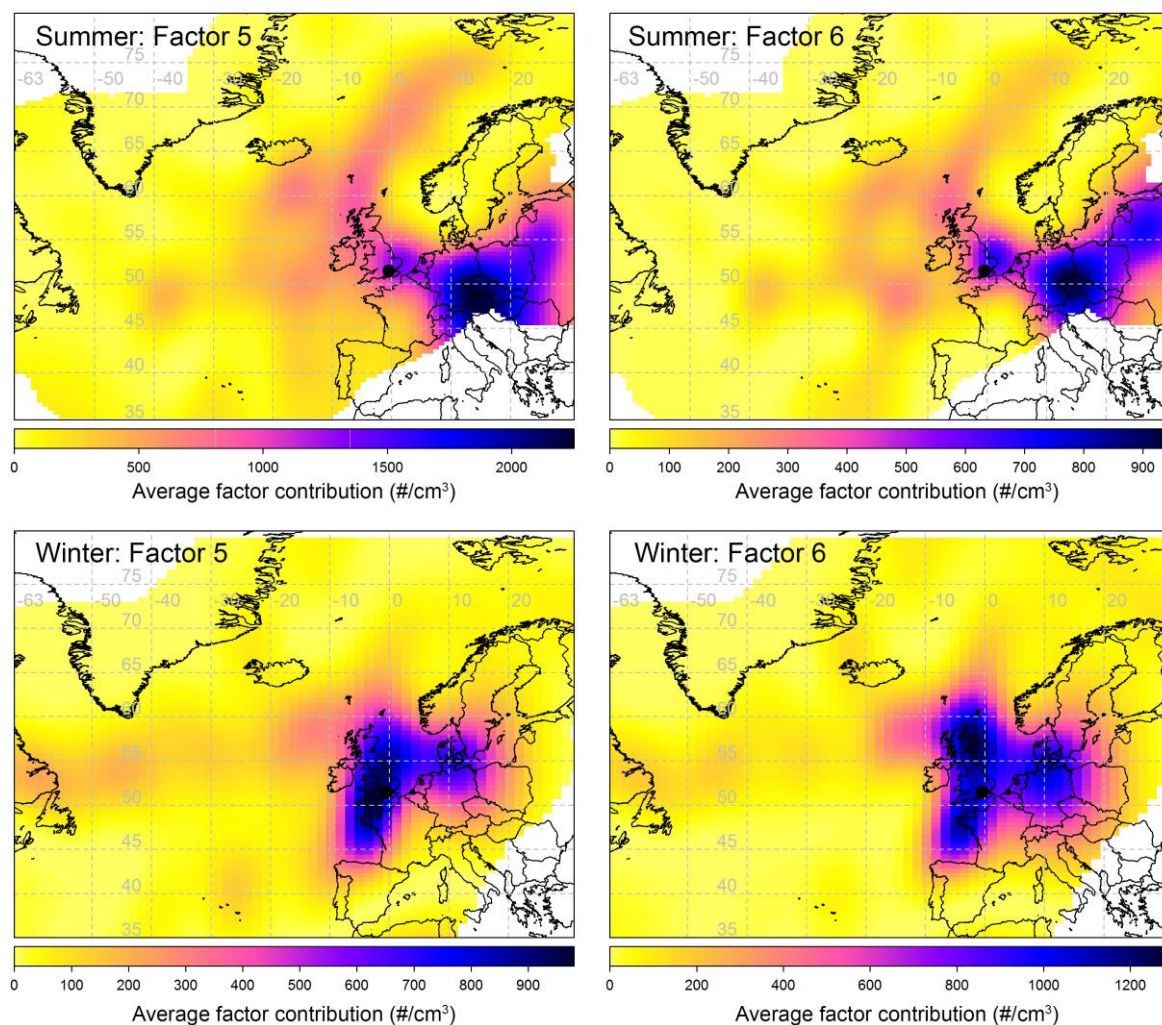


Figure 7. CWT maps of the secondary aerosol-related factors for both the seasons. Map scales refer to the average factor contributions to the total variable (PNC).

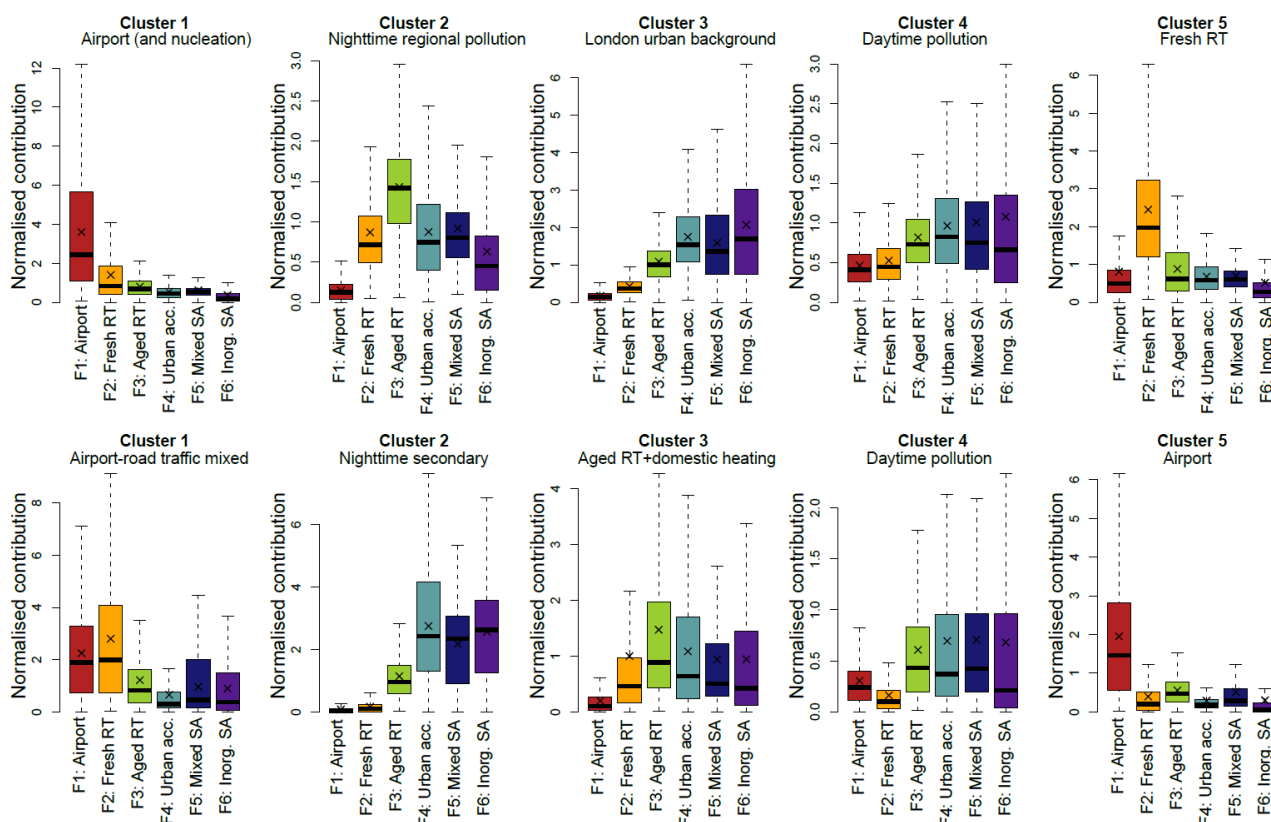


Figure 8. Comparison of k-means and PMF for the warm (upper plots) and cold (bottom plots) seasons. Boxplot statistics: lines= medians, crosses= arithmetic means, boxes= 25th-75th percentile ranges, whiskers= $\pm 1.5 \times$ inter-quartile ranges.

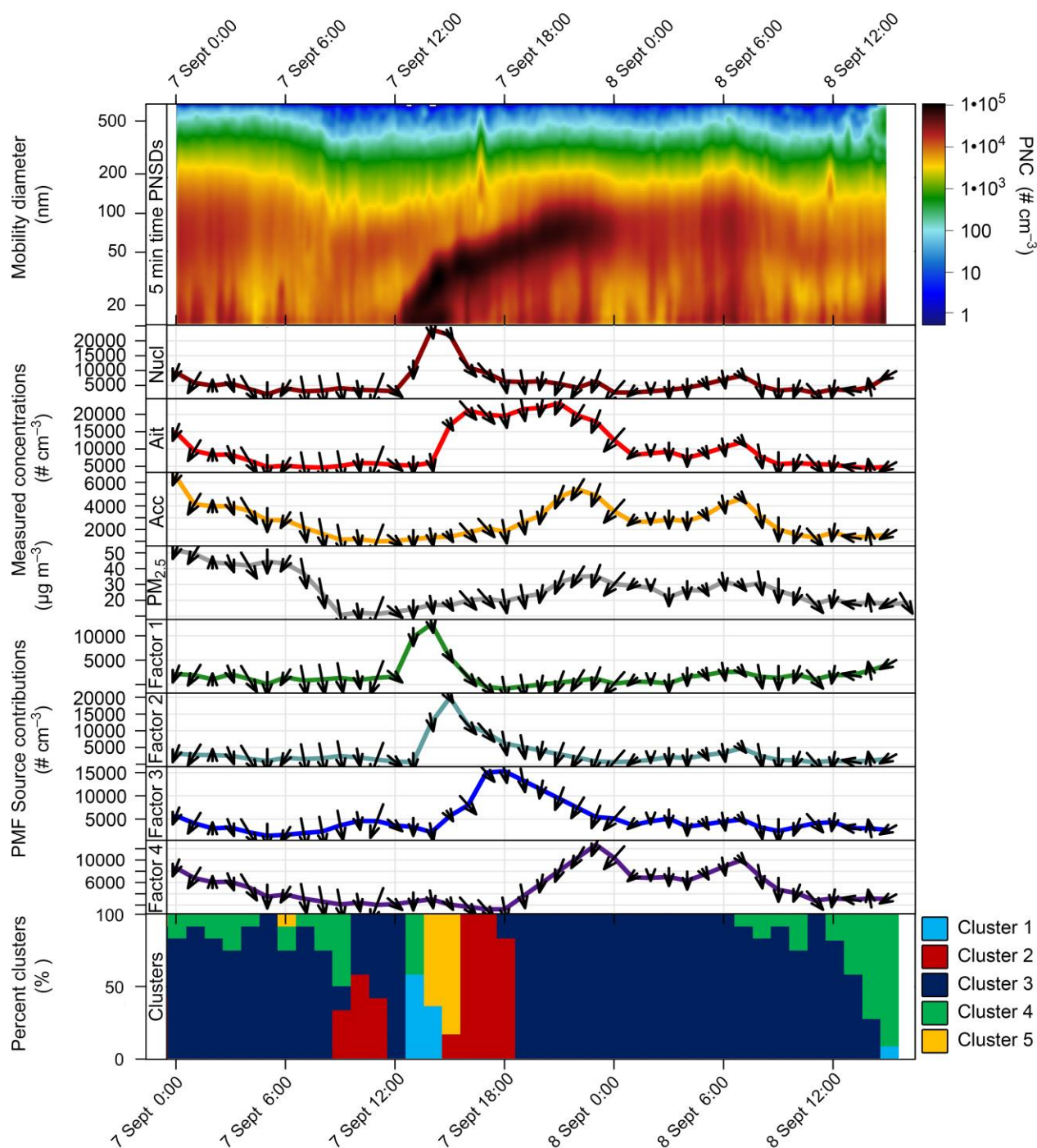


Figure 9. Analysis of the regional nucleation episode occurring on September 7th. The selected period is from 7 September midnight to 8 September 4 pm. The plots represent (from upper to the bottom): (a) contour plots of SMPS data; (b) Concentrations of some measured species (Nucl= particles in the nucleation range 14-30 nm; Ait= particles in the Aitken Nuclei range 30-100 nm; Acc= particles in the accumulation range >100 nm; mass of PM_{2.5}); (c) Source contributions from PMF for the Factors 1, 2, 3 and 4; (d) hourly counts of number of clusters. The arrows in the (b) and (c) plots show the wind direction (arrow direction) and speed (proportional to arrow length).